Accurate Ensemble Molecular Dynamics Binding Free Energy Ranking of Multidrug-Resistant HIV-1 Proteases

S. Kashif Sadiq, David W. Wright, Owain A. Kenway, and Peter V. Coveney*

Centre for Computational Science, Department of Chemistry, University College London, London, WC1H 0AJ, United Kingdom

Received January 5, 2010

Accurate calculation of important thermodynamic properties, such as macromolecular binding free energies, is one of the principal goals of molecular dynamics simulations. However, single long simulation frequently produces incorrectly converged quantitative results due to inadequate sampling of conformational space in a feasible wall-clock time. Multiple short (ensemble) simulations have been shown to explore conformational space more effectively than single long simulations, but the two methods have not yet been thermodynamically compared. Here we show that, for end-state binding free energy determination methods, ensemble simulations exhibit significantly enhanced thermodynamic sampling over single long simulations and result in accurate and converged relative binding free energies that are reproducible to within 0.5 kcal/mol. Completely correct ranking is obtained for six HIV-1 protease variants bound to lopinavir with a correlation coefficient of 0.89 and a mean relative deviation from experiment of 0.9 kcal/mol. Multidrug resistance to lopinavir is enthalpically driven and increases through a decrease in the protein−ligand van der Waals interaction, principally due to the V82A/I84V mutation, and an increase in net electrostatic repulsion due to water-mediated disruption of protein−ligand interactions in the catalytic region. Furthermore, we correctly rank, to within 1 kcal/mol of experiment, the substantially increased chemical potency of lopinavir binding to the wild-type protease compared to saquinavir and show that lopinavir takes advantage of a decreased net electrostatic repulsion to confer enhanced binding. Our approach is dependent on the combined use of petascale computing resources and on an automated simulation workflow to attain the required level of sampling and turn around time to obtain the results, which can be as little as three days. This level of performance promotes integration of such methodology with clinical decision support systems for the optimization of patient-specific therapy.

INTRODUCTION

The free energy change of biomolecular association is arguably one of the most important physical quantities in biochemistry, governing the myriad processes that occur in living organsims as well as being one of the pivotal determinants in biomedical therapy and pharmaceutical activity.[1,2] A variety of well-established experimental methods exist to determine free energies of binding, especially for enzyme−ligand complexes,[3,4] including their constituent enthalpic and entropic components,[5,6] but these are neither feasible nor economical to implement in a high-throughput manner.

Within the framework of molecular dynamics simulation, several well established computational approaches also exist to compute binding free energies.[7] Many of these methods are either rapid but less accurate, usually requiring empirical fitting first, as in the linear interaction energy (LIE) method,[8,9] or accurate but extremely slow, such as free energy perturbation (FEP),[10] thermodynamic integration (TI),[11] and umbrella sampling (US).[12] Some methods, such as the molecular mechanics Poisson−Boltzmann surface area (MMPBSA) continuum solvent method,[13−16] strike a compromise between accuracy and speed.

However, there are principally two limiting problems with all such computational approaches: (i) a restricted accuracy in the interatomic potential energy force field and model method used and (ii) an insufficient capacity to sample the significant ensemble of microstates of a system that form the thermodynamic binding free energy, resulting in excessively long convergence times. Furthermore, even methods that compute accurate relative binding free energies between similar complexes, like FEP and TI, are still unappealing due to hitherto largely unattainable computational requirements.

Sampling is also limited by the tendency of single MD simulations to become trapped in local energetic minima for long periods of simulated time. Multiple/ensemble MD approaches have been shown to overcome such barriers.[17] Typically each member of an ensemble is initiated with a randomly seeded velocity distribution, allowing for the exploration of differing regions of phase space, thus facilitating greater sampling of phase space than that available through a single simulation.

Using recently developed distributed compute resources, like those utilized by the Folding@home project,[18] such types of approaches have been applied to problems of protein folding and membrane fusion[19,20] and to binding free energy calculations using accurate methods like FEP.[21,22] However, they have had limited success in correctly distinguishing relative binding free energies between slightly varying

* Corresponding author e-mail: p.v.coveney@ucl.ac.uk.

10.1021/ci100007w
Published on Web 04/12/2010

complexes requiring sensitive discrimination below 0.5 kcal/mol. Furthermore, a quantitative thermodynamic comparison between the effectiveness of the ensemble approach compared to the single-trajectory approach has not been carried out.

In recent years, the MMPBSA method has received much attention because of the appeal of determining absolute binding free energy differences through computing equilibrium end-state differences via alternative thermodynamic pathways, instead of the inaccessible route of completely sampling protein−ligand binding events in solution. However, the method poses several limitations for computing absolute binding free energies. First, it does not implicitly account for free energy differences that arise due to conformational changes upon binding, possible changes in key protonation states, and changes due to explicit water-mediated binding between protein and ligand. Furthermore, an additional non-negligible component needs to be incorporated into the calculation to determine the change in configurational entropy upon ligand binding.

We have previously shown that approximate methods, like MMPBSA, using the single-trajectory approach can in principle yield accurate discrimination of binding free energies to within 1.5 kcal/mol but require an appropriate choice of starting structures and sampling trajectories.[16] The recent emergence of closely coupled high-performance computing resources at the 'petascale' (a sustained performance of the order of petaflops and comprised of many tens to hundreds of thousands of cores) now allows the problem of sampling to be more rigorously assessed.

The key question we address here is whether relative protein−ligand binding free energies can be distinguished to a sufficient degree of accuracy by an enhancement of the MMPBSA method, within a computational sampling time that precludes the appeal of utilizing more exact methods. We investigate a wild-type and five multidrug-resistant (MDR) HIV-1 proteases bound to the widely used inhibitor lopinavir as well as the cross-drug comparison of the wild-type with the first-generation inhibitor saquinavir.

We have chosen these systems for several reasons. First, the method we employ here provides a rigorous investigation of relative free energies of mutants whose binding affinities can vary by less than 0.5 kcal/mol, thus providing a sensitive test of the method. Second, by comparing two different drugs bound to the wild-type protease, we are able to investigate whether the method allows effective drug ranking. Finally, our investigation provides a rigorous assessment of the absolute binding free energy for same-state unbound to same-state bound proteases. However, as well as exhibiting significant changes in configurational entropy, the HIV-1 protease exhibits a wide array of state changes upon ligand binding, stemming partially from the well characterized flexibility of the enzyme[23,24] and enzyme−ligand complex.[25] These comprise significant conformational changes of the β-hairpin flaps upon binding,[26−29] changes in the likely protonation states between unbound and bound forms,[30] and changes in the introduction of water molecules that mediate protein−ligand interactions in the active site.[31,32] Each of these phenomena contribute significantly to the absolute binding free energy[33−36] and thus need to be summed as a correction factor. We estimate this correction factor based on calculations from an array of previous studies and compare this with the deviation of our simulations from the experimental absolute binding free energy.

Using the above systems, an ensemble molecular dynamics protocol is applied to the MMPBSA methodology and compared against single long trajectories. We show that the ensemble method is necessary to achieve correctly distributed and converged sampling of conformational microstates. Recently, moderately accurate absolute binding free energies were determined for a peptide substrate binding to HIV-1 protease, requiring μs time scale biased metadynamics sampling in explicit solvent.[37] We, therefore, exhaustively sample the MMPBSA end-state thermodynamic method up to the computational limit for HIV-1 protease, corresponding to 1 order of magnitude less than more exact methods. At such a time scale, and by applying ensemble methods to achieve correct and adequate sampling of conformational microstates, we find that accurate relative binding free energy ranking is possible, independent of choosing a closely matching starting structure or optimizing trajectory selection. By performing a reproducibility study of selected systems, we also determine the limit of accuracy of this methodology.

Furthermore, we discuss the extent to which the ensemble approach is additionally advantageous over the single-trajectory approach in terms of massively reducing the wall-clock time for computing a free energy, given adequate computing resources. Rapid and accurate turn around of an array of binding free energies is crucial for enhancing patient-specific clinical decision support.[38] We show how the concerted use of petascale computing resources, the appropriate free energy methodology, adequate sampling, and an automated workflow[39] make turn around feasible within three days. Finally, the clinical and therapeutic relevance of investigating drug resistance in HIV-1 protease is paramount for enhancing rational drug design as well as optimizing patient-specific therapy,[38,40−42] in the light of the complex mutational pathways that exist for the enzyme.[43−45]

METHODS

We performed fully atomistic molecular dynamics simulations and subsequent binding investigations of six HIV-1 proteases complexed with the widely used FDA approved inhibitor lopinavir (LPV) using two simulation strategies: (i) single simulations up to 50 ns production each, termed 1 $\times$ 50 ns hereafter and (ii) ensembles of 50 shorter simulations up to 1 ns production each, termed 50 $\times$ 1 ns hereafter. The latter were extended to 4 ns production each, termed 50 $\times$ 4 ns hereafter. In addition we simulated wild-type HIV-1 protease with the inhibitor saquinavir (SAQ), using the 50 $\times$ 4 ns ensemble approach in order to provide a cross-drug thermodynamic comparison and ranking. HIV-1 protease is a homodimer with C_2-symmetry and a monomeric chain length of 99 amino acids (see Figure 1). A single dimeric mutation corresponds to two amino acid mutations, one at each identical position along the monomer. The consensus wild-type selected for this study was the HXB2 sequence. Alongside the HXB2 wild-type, we investigated five mutants corresponding to those previously studied experimentally by Ohtaka et al.[6] and comprising subsets of a complete set of six MDR mutations, namely L10I, M46I, I54V, V82A, I84V and L90M. For brevity, each mutant was assigned a code name (see Table 1).

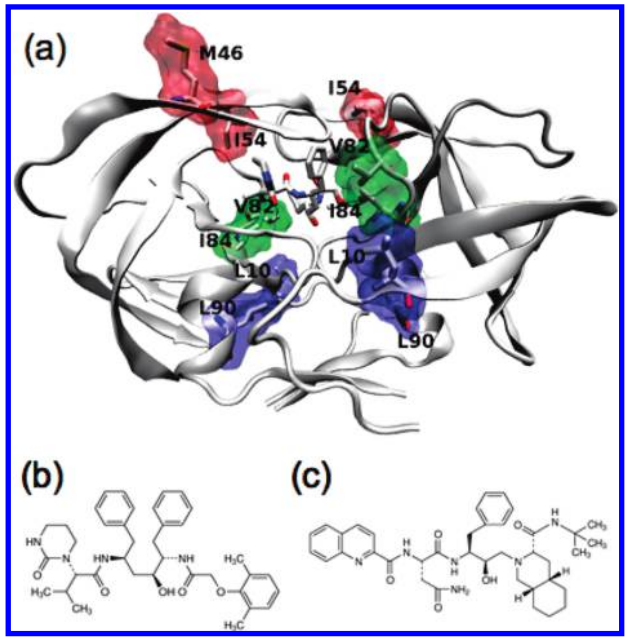

Figure 1. (a) HIV-1 protease (backbone shown in ribbon representation) bound to the inhibitor lopinavir (shown in chemical structure representation). Positions at which the multidrug-resistant (MDR) mutations, studied here, occur are shown in chemical structure and space-filling representation. The active site (AS) mutations V82A/I84V are shown in green, the dimer mutations (DM) L10I/L90M in blue, and the flap (FL) mutations M46I/I54V in red. Chemical structures of (b) lopinavir (LPV) and (c) saquinavir (SAQ) are also shown.

Table 1. Code Name and Mutational Composition of HIV-1 Protease Sequences Investigated

code	description	mutations
WT	wild-type	HXB2
HM	MDR hexa mutant	L10I, M46I, I54V, V82A, I84V, L90M
QM	MDR quatro mutant	M46I, I54V, V82A, I84V
AS	active site mutant	V82A, I84V
FL	flap mutants	M46I, I54V
DM	dimer interface mutants	L10I, L90M

The study reported here extended over 250 ns of production per system (~40 000 atoms), ~2 μs in total, and was 20-fold larger than the previous largest study on HIV-1 protease binding using a similar method.[16] Such sampling was unachievable realistically without a concerted use of large petascale compute resources and an automated molecular simulation framework, such as the Binding Affinity Calculator (BAC),[39] a molecular simulation/free energy calculation workflow tool integrated with the Application Hosting Environment[46] middleware, used herein.

Initial Preparation and Simulation Protocol. Initial preparation of all systems, production molecular dynamics simulations, and postprocessed free energy calculations were implemented using BAC.[39] The full details of the methodology and protocol are provided in Sadiq et al.[39] and Stoica et al.,[16] but specific details are additionally described here for convenience.

Protease and ligand coordinates were extracted from the 1MUI crystal structure into separate files. Missing hydrogens were inserted on drug coordinates using the PRODRG tool.[47] Gaussian 03[48] was used to perform geometric optimization of all inhibitors at the Hartree−Fock level with 6-31G** basis functions. The restrained electrostatic potential (RESP) procedure, which is part of the AMBER9 package,[49] was used to calculate the partial atomic charges. The Visual Molecular Dynamics (VMD) package[50] was used to incorporate protease mutations, to insert all missing protease hydrogens, and to assign the protonation state of the catalytic dyad. The force field parameters for the inhibitors were completely described by the general AMBER force field (GAFF).[51] The standard AMBER force field for bioorganic systems (ff03)[52] was used to describe the protein parameters as well as those for the natural substrates. It is well established from the many crystal structures of ligand-bound HIV-1 protease complexes that a water molecule mediates β-hairpin flap−ligand interactions.[53] Strangely, the 1MUI crystal structure has not resolved this crucial water molecule. Therefore, a water molecule was inserted in the correct tetrahedrally coordinated flap−ligand cavity. The Leap module[54] in the AMBER 9 software package was then used to combine each apo-protease system with the ligand and the inserted water molecule, to electrically neutralize each ligand-bound system, and to solvate using atomistic TIP3P water[55] in a cubic box with at least 14 Å distance around the complex, resulting in a fully atomistic system of approximately 40 000 atoms for each system.

Minimization was conducted using the conjugate gradient and line search algorithms available in NAMD2[56] for 2000 iterations. The long-range Coulomb interaction was handled using the particle mesh Ewald summation method (PME).[57] A nonbonded cutoff distance of 12 Å was used for all simulations. For the equilibration and subsequent production runs, the SHAKE algorithm[58] was employed on all atoms covalently bonded to a hydrogen atom, allowing for an integration time step of 2 fs. The system was gently annealed from 50 to 300 K over a period of 50 ps and then maintained in the isothermal−isobaric ensemble (NPT) thereafter at a target temperature of 300 K and target pressure of 1 bar, using a Langevin thermostat and Berendesen barostat,[59] respectively, with a restraining force constant of 4 kcal/mol/Å^2 on all heavy atoms. The system was then equilibrated for 200 ps at 300 K to ensure thorough solvation of the complex and to prevent premature flap collapse.[60] Sequentially, the heavy atoms of each dimeric mutation and those of amino acids within a 5 Å surrounding region were completely relaxed for a duration of 50 ps each after which the heavy atoms of that region were again constrained by a force of 4 kcal/mol/Å^2. This procedure was followed by a gradual force reduction on the ligand from 4 to 0 kcal/mol/Å^2 over a 200 ps period in equal stages of 1 kcal/mol/Å^2 and then a similar force reduction on the protease from 4 to 1 kcal/mol/Å^2 over a period of 150 ps. In the final stage of equilibration, all constraints were removed from the protease, and the system was allowed to evolve completely unrestrained up to a total duration of 2 ns. The production simulations for each system were also performed in the isothermal−isobaric ensemble (NPT), described above, each for a duration of 50 ns. The coordinates of the trajectories were recorded every 1 ps throughout all equilibration and production runs. The only initial variation in each replica of the same system was the randomly seeded velocity distribution assigned to the atoms of the system.

Free Energy Calculation Protocol. The absolute free energy difference of binding ΔG_{theor} is given by

$$\Delta G_{\text{theor}} = \langle \Delta H_{\text{theor}} \rangle_M - T \langle \Delta S_{\text{theor}} \rangle_N \qquad (1)$$

Here, $<\Delta H_{theor}>_M$ denotes the average of the enthalpic part resulting from the MMPBSA calculation over M snapshots, while $<\Delta S_{theor}>_N$ term denotes the average change in configurational entropy resulting from normal mode calculations across N snapshots. Enthalpies and configurational entropies were calculated at a frequency of 100 and 5 snapshots/ns respectively, resulting in $M = 5000$ enthalpy and $N = 250$ entropy snapshots for each 1×50 ns simulation and concatenation of 50×1 ns simulations, and $M = 20\,000$ enthalpy and $N = 1000$ entropy snapshots across each concatenation of 50×4 ns simulations. Each snapshot corresponded to an independent estimate of the binding free energy.

The enthalpic value of each snapshot is given by

$$\Delta H_{theor} = \Delta H_{vdW}^{MM} + \Delta H_{ele}^{MM} + \Delta H_{pol}^{sol} + \Delta H_{nonpol}^{sol} \quad (2)$$

where ΔH_{vdW}^{MM} and ΔH_{ele}^{MM} are the van der Waals and electrostatic contributions to the molecular mechanics free energy difference, respectively, and ΔH_{pol}^{sol} and ΔH_{nonpol}^{sol} are the polar and nonpolar solvation terms, respectively.

The molecular mechanics free energy differences (ΔH_{vdW}^{MM} and ΔH_{ele}^{MM}) were calculated using the SANDER module in AMBER 9, with no cutoff for the nonbonded energies. The AMBER PBSA module was used for the evaluation of the electrostatic free energy of solvation ΔH_{pol}^{sol}. A grid spacing of 0.5 Å was employed for the cubic lattice, the internal and external dielectric constants were set to 1 and 80, respectively, and 1000 linear iterations were performed. The nonpolar solvation free energy ΔH_{nonpol}^{sol} was calculated from the solvent accessible surface area (SASA) using the MSMS program,[61] with a probe radius of 1.4 Å, the surface tension γ being set to 0.00542 kcal/(mol/Å^2), and the offset β to 0.92 kcal/mol.

The changes in configurational entropy upon ligand association ΔS were estimated by an all-atom normal-mode analysis performed with the AMBER NMODE module. Prior to the normal-mode calculations, the complex, receptor, and ligand were subjected to minimization with a distance-dependent dielectric constant $\varepsilon = 4r$ and a convergence tolerance tighter than drms $= 10^{-4}$ kcal/mol/Å.

Although the study reported here is principally motivated by the effect of differential sampling on free energy, the choice of parameters used in the model construction and the MMPBSA method also affects the computed binding free energy. For example, the choice of protonation state of the catalytic aspartyl dyad in the bound-state of the protease will have substantial effects and is discussed herein. Also, as noted in our previous study,[16] the choice of internal dielectric constant can effect the calculation of polar solvation energies. Previous MMPBSA calculations have used values in the range of 1−4 for the dielectric.[14,62,63] We assigned a dielectric of 1 based on our previous assessment,[16] in which we found significant deviation of free energies away from experimental results for increases away from this default value. In addition to this, choice of the surface tension term will affect the nonpolar component of solvation. However, based on previous studies of nonpolar solvation,[64] there is substantial motivation for choosing the well-established values for γ and β assigned here. The advantage of choosing default values derived by independent methods is that it further tests the accuracy of our method.

Convergence Analysis Methods. Convergence of free energies was assessed by a number of methods, extending those reported by Stoica et al.[16] First, the extent to which each data set described a Gaussian distribution was determined. Second, the root-mean-squared (RMS) difference between the forward ($<\Delta X>_\tau^{for}$) and reverse ($<\Delta X>_\tau^{rev}$) cumulative means along the trajectories $\sigma(\varepsilon)$ was calculated such that:

$$\Delta\Delta X_\tau = <\Delta X>_\tau^{for} - <\Delta X>_\tau^{rev} = \frac{1}{\tau}\left[\sum_{i=1}^{\tau}\Delta X_i - \sum_{i=N-\tau+1}^{N}\Delta X_i\right] \quad (3)$$

where X denotes either enthalpy (H) or entropy (S), i is the ith snapshot, τ is the number of snapshots over which the mean was taken, N is the total number of snapshots analyzed, and $\Delta\Delta X_\tau$ is the instantaneous difference, giving:

$$\sigma(\varepsilon) = \sqrt{\frac{1}{\omega}\sum_{j=\varepsilon}^{\varepsilon-1+\omega}\Delta\Delta X_j^2} \quad (4)$$

where ε is the number of snapshots into a trajectory, and ω is the number of snapshots over which the RMS difference was calculated, set to 1 ns or $\omega = 100$ and $\omega = 5$ for enthalpy and entropy, respectively. Comparison between the first and second half of a trajectory is represented by $\sigma(N/2)$ and thus the maximum sample size for completely nonoverlapping data sets. By definition, beyond this, the value of $\sigma(\varepsilon)$ decays and is 0 at the point of complete equivalence of trajectories. Therefore, $\sigma(\varepsilon)$ was calculated only to the halfway point.

Assignment of Protonation State. Prior to a calculation of the binding free energies of the mutant complexes, the protonation state of the catalytic dyad (D25/D25′) when complexed to lopinavir was investigated using the MMPBSA methodology. These states were then used to assign the protonation states of each of the corresponding mutant−lopinavir complexes. The protonation state of saquinavir was assigned in accordance with our previous study.[16] Four systems, each consisting of a different catalytic−dyad protonation state were generated for the wild-type−lopinavir complex. These were denoted as the dianionic (D-), diprotonated (D25, D25′), Asp 25 protonated (D25), and Asp 25′ protonated (D25′) states. Ensemble production simulations were performed up to 20×4 ns for each system (except for D-, for which 10×4 ns were performed), and results were computed at the frequency mentioned above.

The protonation state of the dyad is the subject of much uncertainty, and there have been many studies investigating it (see ref 65 and references therein). While optimal catalytic activity correlates with a slightly acidic pH in the range 5−6,[66] at physiological pH, the protease is unprotonated. Furthermore, the protease may even make use of different protonation states to maintain activity while transitioning from physiological intracellular to slightly acidic intravirion environments. In addition to this, when bound to inhibitors, the chemical specificity of the ligand near the dyad may play an important role in determining the subsequent dyad protonation state.[67]

In Table 2, we present the MMPBSA calculated ligand binding free energies for each protonation state of the

Table 2. Assessment of Catalytic Dyad Protonation State for Wild-Type HIV-1 Protease Bound to Lopinavir From a 20 × 4 ns Ensemble[a]

Protonation state	ΔH	$-T\,\Delta S$	ΔG_{bind}
D25	–47.70 (0.05)	37.29 (0.79)	–10.41 (0.84)
D25′	–46.13 (0.05)	38.92 (0.80)	–7.21 (0.85)
D25, D25′	–47.67 (0.05)	39.85 (0.83)	–7.82 (0.88)
D-	–32.15 (0.11)	38.23 (1.23)	6.08 (1.34)

[a] D- is from a 10 × 4 ns ensemble. Mean energies are in kcal/mol. Standard errors are shown in parentheses.

catalytic Asp dyad as well as decomposed enthalpic and entropic contributions. It should be emphasized that, as noted by Wittayanarakul et al.,[30] these calculations do not take into account the energetic cost of changing the protonation state of the enzyme upon ligand binding, from the assumed D25 state of the apo-protease. Therefore, following the argument of Wittayanarakul et al.,[30] our predictions permit an accurate comparison only for the monoprotonated states. Based on our results, the D25 protonation state for the dyad was assigned due to it exhibiting a substantial minimum in both the free energy of binding as well as the enthalpic component of binding, as compared to the other systems.

Computational Infrastructure and Performance. The Ranger machine (with 62 976 cores) at the Texas Advanced Computing Center (TACC) was used for the production simulations. The optimally scaled rate of computation was approximately 8 h/ns on 32 opteron cores/replica. Minimum single-trajectory turn around time (TAT) using 192 cores (at 18 ns/day) was 416 h; theoretical minimum ensemble trajectory TAT using 9600 cores (simulating 300 replicas simultaneously at 900 ns/day) was 48 h. In practice, we achieved on average 120 ns/day with a peak of 300 ns/day. MMPBSA and normal-mode post processing took 3 and 20 h/ns, respectively, but was run in parallel for each nanosecond using the Leeds node (256 cores) of the U.K. National Grid Service. The theoretical minimum total turn-around time (simulation + calculation) using this approach was thus approximately three days.

INTERNAL SAMPLING, CONVERGENCE, AND REPRODUCIBILITY

In order to compare the sampling and convergence properties of single and ensemble trajectories, we analyzed both the extent of Gaussian sampling and the convergence between the forward and reverse cumulative means achieved by each methodology, specifically for 1 × 50, 50 × 1 and 50 × 4 ns trajectories. As large instantaneous variations are inherent to both the MMPBSA and the normal-mode methods,[16] 1 ns running averages were also determined. These, together with the forward and reverse cumulative means for each method, are provided in Figures 1−3 in the Supporting Information. Here, we report the degree of convergence exhibited by each method by analyzing the RMS difference between the forward and reverse cumulative means $\sigma(\varepsilon)$ and additionally investigate the extent of energetic sampling, as compared to structural sampling. Furthermore, we determine an overall estimate of the statistical error in the method by performing a reproducibility study of the 50 × 4 ns method for the WT and HM systems.

Single versus Ensemble Trajectories. Figure 2 shows the normalized frequency distribution for (a) enthalpic and (b) entropic components of binding for both 1 × 50 and 50 × 1 ns trajectories (red and blue points, respectively) for each MDR system. For the enthalpic component of binding (see Figure 2a), substantial differences were observed between the 1 × 50 and 50 × 1 ns trajectories. In all MDR systems, the mean enthalpy of the 1 × 50 ns trajectory distribution varies from that of the 50 × 1 ns distribution by approximately 1 and 16 kcal/mol. The difference in the mean enthalpic values from the 1 × 50 ns trajectories is greater than that from the respective 50 × 1 ns trajectories for all systems, except the wild-type. Furthermore, the 1 × 50 and 50 × 1 ns standard deviation of enthalpies for the WT, DM, and FL systems is similar (see Methods Section for definitions of protease systems), while the 1 × 50 ns simulations exhibit greater standard deviations for the FL and AS systems than the respective 50 × 1 ns trajectories. For both 1 × 50 and 50 × 1 ns trajectories, most data sets exhibit an approximately normal distribution albeit with several exceptions exhibited in the 1 × 50 ns simulations. Most noticeably, the forms of the 1 × 50 ns trajectory distributions for AS and QM do not resemble that of a Gaussian distribution. Indeed, several peaks in the distribution are observed for the AS system at approximately −45 and −37 kcal/mol and for the QM system at approximately −26 and −28 kcal/mol, indicating that, in these two systems, specific energy minima are sampled for a statistically inadequate period of time. In contrast, all 50 × 1 ns simulations exhibit an approximately normal distribution, indicating that all energy minima are sampled correctly.

Analysis of the configurational entropy shows greater similarity between the sampling achieved by the 1 × 50 ns trajectory as compared to that of the 50 × 1 ns trajectory runs (see Figure 2b). Both the 1 × 50 and the 50 × 1 ns trajectory runs sample the full range of available $-T\Delta S_{theor}$ values, ranging between approximately 80 to 0 kcal/mol. The entropic component of binding exhibits signficantly different sampling behavior to that of the enthalpic component for both 1 × 50 and 50 × 1 ns trajectory runs. First, several data points do not lie on the expected normal distribution curve for the given mean and standard deviation of the respective data set. Instead there are slight deviations in all systems either above or below the expected normal curve as well as separation of modal minima from the mean. This indicates that the entropy values are favorably distributed around a smaller subset of specific minima and that some values of entropy are less accessible for particular systems.

In the WT system, the entropic minimum for the 50 × 1 ns trajectories is 5 kcal/mol less positive than the mean. In the DM system, a wider entropic plateau is exhibited for both 1 × 50 and 50 × 1 ns systems. In the FL system, the modal minima is over 10 kcal/mol more negative than the mean for the 1 × 50 ns trajectory system. In the QM system, the modal minima for the 1 × 50 and 50 × 1 ns trajectories is more positive by 15 and 5 kcal/mol, respectively, and in the AS and HM systems, the modal values for the 50 × 1 ns trajectories coincide with the mean values but with a larger frequency distribution. Additional minor minima are all also exhibited in a number of systems relatively distant from the mean. Frequency distribution analysis thus indicates the existence of a subset of conformational minima into which normal-mode analysis places various initial conformations.

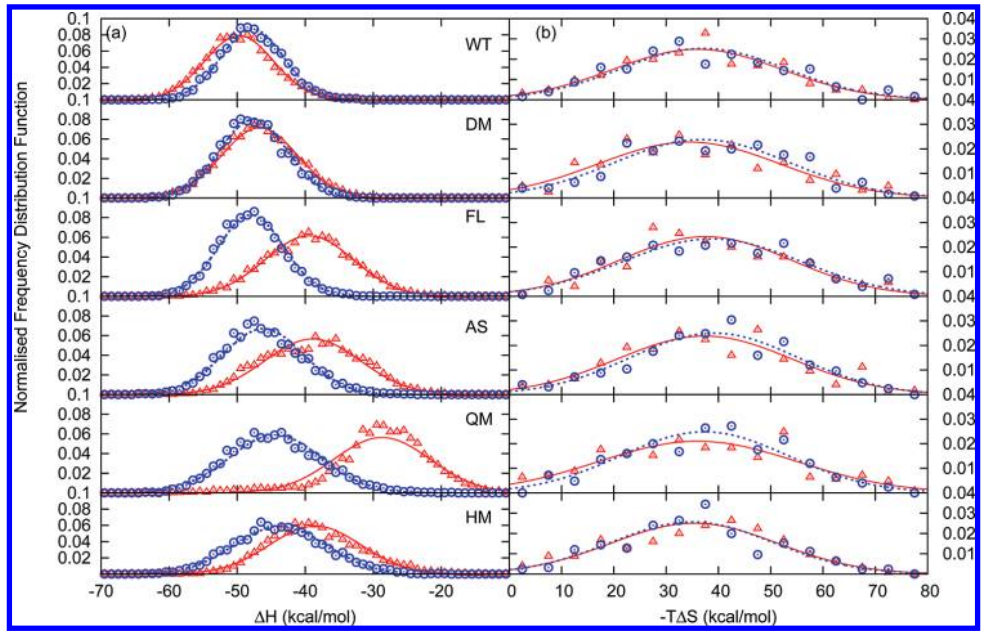

Figure 2. Normalized frequency distribution analysis for (a) enthalpic and (b) entropic components of binding for the 1 × 50 ns (red triangles) and 50 × 1 ns trajectories (blue circles) for each MDR system. The expected normal distribution given the same mean and standard deviation for each data set is shown by the red and blue lines, respectively. The WT, DM, FL, AS, QM, and HM systems are defined in the Methods Section (see Table 1).

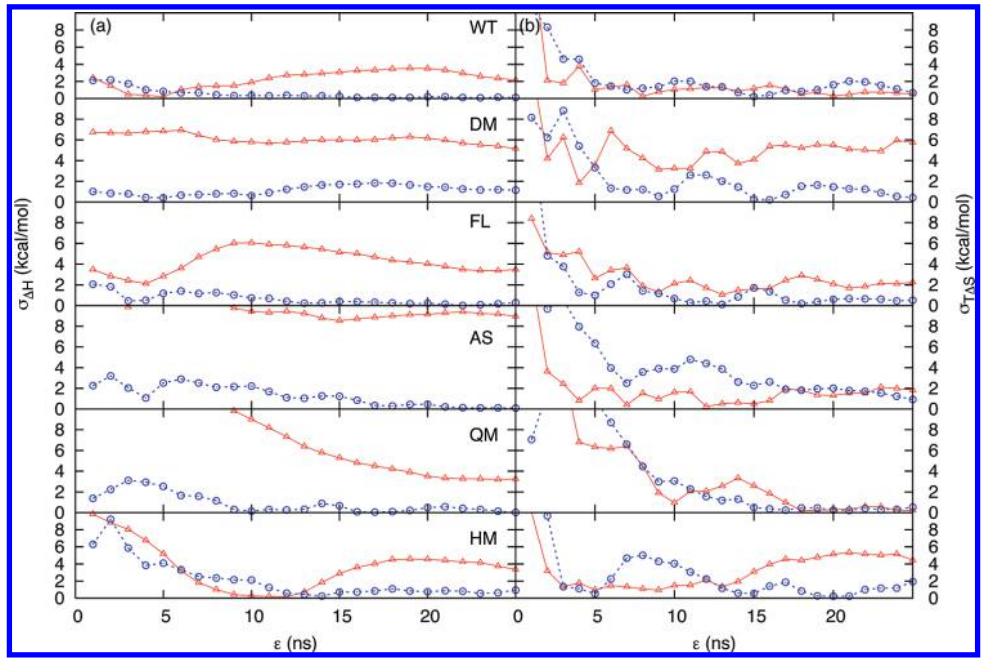

Figure 3. RMS difference in cumulative means $\sigma(\varepsilon)$ of the (a) enthalpic component of binding and (b) entropic component of binding for 1 × 50 ns trajectories (red lines) and concatenated 50 × 1 ns trajectories (blue lines).

Convergence analysis also differentiates the enthalpic sampling of the 1 × 50 ns trajectories as compared to the 50 × 1 ns trajectories. In the 1 × 50 ns simulations, the RMS difference in the forward and reverse cumulative means $\sigma(\varepsilon)$ is larger than 2 kcal/mol up to 25 ns into the simulations (see Figure 3a) for all systems and is as large as 9 and 5 kcal/mol for the AS and DM systems, respectively. This is indicative of the latter portions of each trajectory consistently sampling different energy minima to that of the first part of the trajectory (see Figures 1−3 in the Supporting Information). However, the difference consistently falls below 1.5 kcal/mol within 25 ns into each concatenated 50 × 1 ns trajectory and is below 0.5 kcal/mol for the WT, FL, AS, and QM systems. This is indicative of statistically relevant sampling of the different energy minima independent of which set of replicas are used.

By contrast, convergence of the configurational entropy, $\sigma(\varepsilon)$ is, in general, more comparable between the 1 × 50 ns and the 50 × 1 ns trajectories, although in some systems, the 50 × 1 ns sampling converges to a lower value than that of the 1 × 50 ns trajectories, being reduced to less than 0.5 kcal/mol at 25 ns, except for AS and HM which both reach a threshold of approximately 2 kcal/mol (see Figure 3a). The 1 × 50 ns trajectories compare to 50 × 1 ns trajectories for the WT, AS, and QM systems, while for the other systems, $\sigma(\varepsilon)$ does not fall below 2 kcal/mol by 25 ns into the trajectory, and DM and HM remain as large as 6 and 4 kcal/mol, respectively.

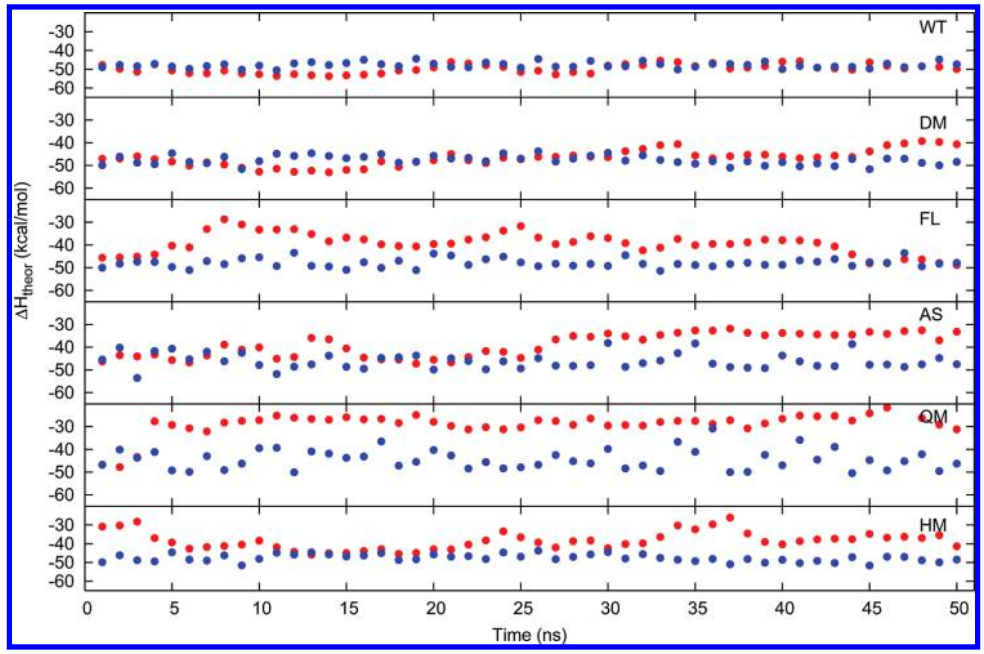

Figure 4. Comparison of the mean enthalpy of binding (< ΔH_{theor} >) for each 1 ns of the 1 × 50 ns trajectories (red) with the mean of each 1 ns member of the 50 × 1 ns trajectories (blue).

Together the normalized frequency distribution and the $\sigma(\varepsilon)$ metric, employed for determining convergence, are able to distinguish trajectories for which Gaussian sampling as well as internally convergent behavior is exhibited. No 1 × 50 ns trajectory run exhibits both correctly sampled and convergent enthalpies even though the WT system appears to. By contrast, all 50 × 1 ns systems exhibit correctly sampled enthalpies that converge to below 1 kcal/mol, within 25 ns of concatentated sampling. Neither the 1 × 50 ns trajectory nor the 50 × 1 ns trajectories exhibit Gaussian sampling of configurational entropies despite convergence to within 2 kcal/mol in the latter.

Structural vs Energetic Sampling. The extent and applicability of structural sampling exhibited by each method was also explored by calculating the root-mean-squared deviation (RMSDs) of the protease backbone relative to the average structure. All 1 × 50 ns and 50 × 1 ns trajectories exhibit stable and comparable RMSDs of around ∼1.5 Å (see Figure 4 in the Supporting Information). Even though the backbone RMSD calculations exhibit similar fluctuations, the degree of difference in structural sampling between the 1 × 50 ns and 50 × 1 ns trajectory methods is not discernible. RMSD measures gross structural sampling, while structural changes important to binding, such as different side chain rotamers, occur on a finer scale. It is likely that the 1 × 50 ns trajectories exhibit greater structural sampling, as the 50 × 1 ns trajectories are only 3 ns away (2 ns equilibration + 1 ns production) from the same starting structure. Complete sampling of the phase space would allow the topology of the free energy landscape to be determined. However, it is well established that the free energy landscapes of protein−ligand interactions are rugged, motivating the use of ensembles of snapshots in the normal-mode method and/or other methods for determining configurational entropy.[68,69] This ruggedness may thus limit the meaning of inferring energy from structural sampling based on single- or even multidimensional reductions of the phase space.

The differences in energetic sampling, however, are discernible. Figure 4 shows a comparison of the mean enthalpy of binding for each 1 ns of the 1 × 50 ns trajectories (red) with the mean of each 1 ns member of the 50 × 1 ns trajectories (blue). A large range of energy values is exhibited in both methods. However, as most notably with the AS and QM systems, the 1 × 50 ns simulations are more susceptible to becoming trapped in local energetic minima, even though they may exhibit greater structural sampling. Conversely, while each individual member of the 50 × 1 ns runs may be similarly affected, the randomized initial velocity distribution causes large energy variations between different members of the ensemble, promoting access to more minima. For example, the AS and QM systems exhibit weaker binding enthalpies in the 1 × 50 ns simulations for long portions of the trajectory. While some individual members of the 50 × 1 ns ensemble sample comparable energy regions, they are infrequent, and instead the ensemble members are distributed across a larger number of energy wells between highest and lowest. As each of the ensemble members is likely to be conformationally closer to the initial structure, this result is consistent with a picture in which the landscape contains several low-energy minima surrounded by high-energy barriers. Such 'calderas' in the landscape need not be distant to the initial structure in the conformational space. It is the combined average of sampling many different energetic regions afforded by the ensemble method that improves convergence.

Extensive structural sampling far from the initial structure is important for free energy methods that gradually integrate changes from one state to another and thus need to sample over the phase space between such states. For these cases, single long trajectory methods may be advantageous as they promote such sampling. In end-state methods such as MMPBSA, the intermediate phase space is not of interest as the method computes the difference between the end states, specifically that of the complex minus the sum of the receptor and ligand components. The conformations of interest are those of the free receptor, the free ligand, and those in which the ligand is categorically bound to the receptor and not on an entry or exit pathway. Previous studies

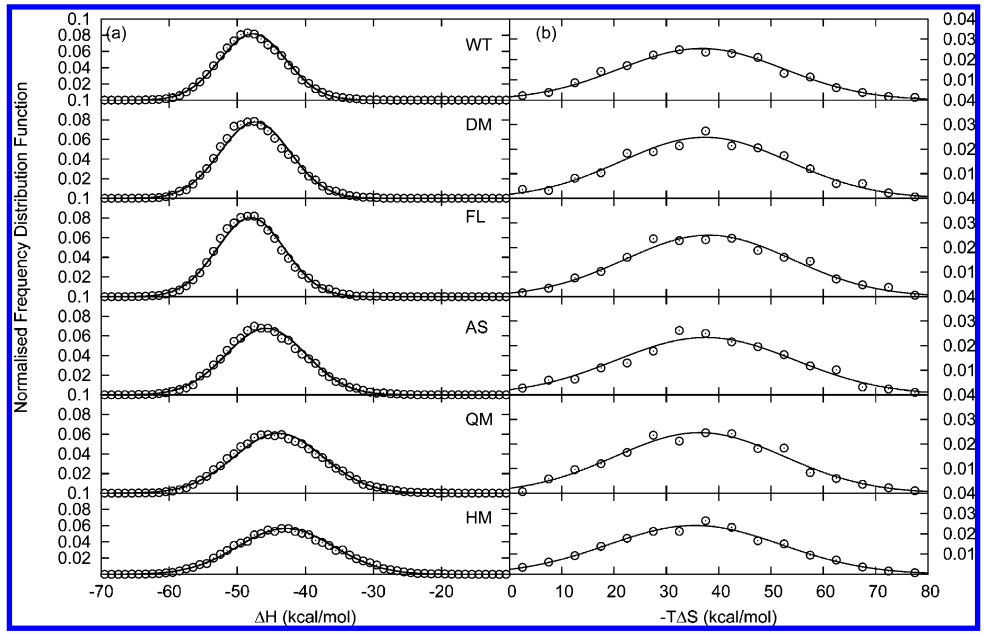

Figure 5. Normal distribution analysis for (a) the enthalpic and (b) the entropic components of binding for the 50 × 4 ns ensemble trajectories for each MDR system. The expected normal distribution, given the same mean and standard deviation for each data set, is shown by the black lines.

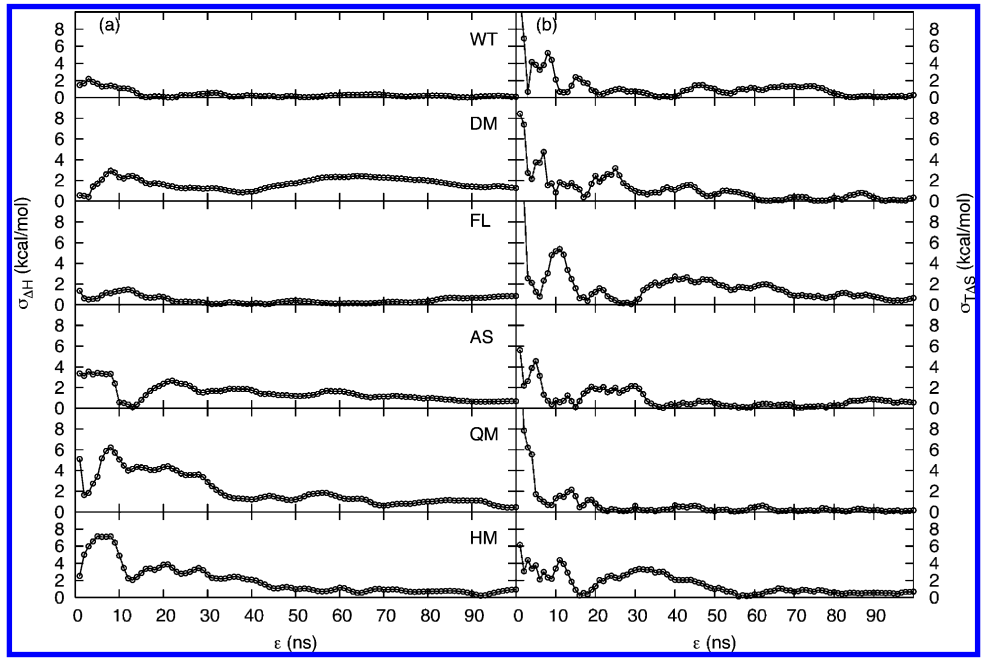

Figure 6. RMS difference in cumulative means $\sigma(\varepsilon)$ for the (a) enthalpic component of binding and (b) entropic component of binding for the concatenated 50 × 4 ns trajectories.

have shown structural drift for inhibitor-bound mutant HIV-1 protease simulations in the multinanosecond regime.[25] The ensemble method is thus especially advantageous for such methods as the shorter time scale of its individual members limit structural drift, while at the same time, promoting enhanced energetic sampling.

Extended Ensemble Sampling and Convergence. To investigate the effects of increased sampling on convergence refinement, all 50 × 1 ns replicas were extended to 4 ns production each, and sampling and convergence properties were examined. Figure 5 shows the normalized frequency distribution for (a) enthalpy and (b) entropy over the extended 50 × 4 ns ensemble trajectories for each MDR system.

All systems exhibit an approximately normal distribution in enthalpy and vary little compared with the distribution attained using 50 × 4 ns trajectories. Similarly the entropy distribution does not improve either at this extended time scale. The small subset of entropic minima sampled are maintained and appeared to be more pronounced even with analysis of 1000 snapshots per system.

Figure 6 shows RMS differences in the forward and reverse cumulative means $\sigma(\varepsilon)$ for (a) enthalpy and (b) entropy. Similar to the properties exhibited by the 50 × 1 ns data set, extension of replicas to 4 ns shows gradual decrease of $\sigma(\varepsilon)$. By 100 ns into the concatenated trajectory (marking the maximum point of nonoverlapping sampling),

the $\sigma(\varepsilon)$ of enthalpy is below 0.5 kcal/mol for all systems, except HM for which a difference of just under 2 kcal/mol is exhibited. Interestingly, the configurational entropy shows even more substantial convergence than the enthalpy; $\sigma(\varepsilon)$ is well below 0.5 kcal/mol for all systems at the midpoint of the simulation.

The results of distribution and convergence analysis reveal important properties of sampling attained using the MMPBSA/normal-mode method. First, single-trajectory simulations do not reliably sample the correct distribution of instantaneous enthalpy values, while ensemble trajectories of the same sample size are shown to sample the distribution better as well as exhibit significantly improved convergence. Second, single and ensemble trajectory methods do not differ substantially in sampling and convergence properties of the normal mode calculation. Distribution analysis reveals a set of local minima around which entropic values cluster. For the systems studied here, averaging over 250 snaphsots (50 ns), neither method is capable of converging results reliably below 1 kcal/mol, although the ensemble method reliably reaches a convergence of 2 kcal/mol. Increasing the sample size in the ensemble method has little effect on the enthalpic calculation as enthalpic values are already converged but does converge the entropic calculation to below 0.5 kcal/mol. The persistent local minima exhibited in the distribution analysis are consistent with the procedure of the normal-mode analysis in which any given snapshot is first minimized in order to diagonalize the Hessian matrix. This causes initially divergent conformations to cluster into the same conformational well, resulting in local clusters of entropic values.

Reproducibility. The extensive convergence and sampling analysis conducted on these HIV-1 protease systems reveals the necessity to use the 50 × 4 ns ensemble method in order to achieve suitably converged enthalpic and entropic values for free energy ranking of such systems. However, it should be noted that, as our results change slightly when going from the 50 × 1 ns to 50 × 4 ns ensemble, further changes may be possible upon extension of the simulation time for each ensemble member. Furthermore, while convergence examines the internal consistency of a data set, a measure of the external error of a free energy prediction can be obtained by comparing multiple identical data sets acquired with the method and the sample time scale to be used for the ranking. We, therefore, performed a reproducibility analysis on the WT and HM systems bound to lopinavir by simulating a second 50 × 4 ns ensemble set for both systems and by comparing them to the original set. As the 50 × 1 ns ensemble is contained within the larger set, this was compared against the previous data too.

The results of the reproducibility analysis are shown in Table 3. The enthalpic and entropic errors exhibited in the 50 × 1 ns WT systems are both within 0.5 kcal/mol, leading to an overall error of 0.43 kcal/mol. The HM system exhibits not only similar enthalpic variation but also an entropic variation of 2 kcal/mol, resulting in a 1.5 kcal/mol difference. Extending to the 50 × 4 ns ensemble insignificantly increases the error between the two WT samples to 0.5 kcal/mol but dramatically decreases the HM error to 0.82 kcal/mol. At this sample size, the relative error between these two systems is, therefore, approximately 1.3 kcal/mol. These results suggest that only the ranking of mutants, whose binding free energies vary above this threshold, can reliably be distinguished, such as QM and HM. However, the HM system exhibits larger entropy fluctuations than the other systems. It is thus likely that a reproducibility study on less resistant mutants, such as AS, may produce similar divergences to the WT result, allowing resistance discrimination within 1 kcal/mol.

Table 3. Reproducibility of Ensemble Investigations for 50 × 1 and 50 × 4 ns Trajectories[a]

sequence	sample	ΔH_{theor}	$-T\Delta S_{theor}$	ΔG_{theor}	$\Delta\Delta G_{II-I}$
		Ensemble (50 × 1 ns)			
WT	I	–47.85(0.05)	36.61(0.68)	–11.24(0.73)	–
	II	–48.33(0.05)	36.66(0.71)	–11.67(0.76)	–0.43(0.76)
HM	I	–43.63(0.10)	34.95(0.98)	–8.68(1.08)	–
	II	–44.16(0.07)	36.98(0.74)	–7.18(0.81)	1.50(1.89)
		Ensemble (50 × 4 ns)			
WT	I	–47.68(0.03)	36.74(0.50)	–10.94(0.53)	–
	II	–48.38(0.03)	36.94(0.51)	–11.44(0.54)	–0.50(1.07)
HM	I	–42.86(0.05)	35.45(0.52)	–7.41(0.57)	–
	II	–43.36(0.05)	36.77(0.52)	–6.59(0.57)	0.82(1.14)

[a] Mean energies are in kcal/mol. Standard errors are shown in parentheses.

Table 4. Computed Free Energy Differences of Binding (ΔG_{theor}) Compared with Experimental Results (ΔG_{exp}) for Wild-Type and All MDR Proteases with LPV Using 1 × 50 ns Single-Trajectory, 50 × 1 ns, and 50 × 4 ns Ensemble-Trajectory Runs and for Wild-Type Binding to Saquinavir Using the 50 × 4 ns Ensemble Trajectory Method[a]

sequence	ΔH_{theor}	$-T\Delta S_{theor}$	ΔG_{theor}	ΔG_{exp}[b]	$\Delta\Delta G_{theor-exp}$[b]
			1 × 50 ns		
WT	–49.72(0.07)	35.85(1.01)	–13.87(1.08)	–15.1(0.09)	1.23(1.17)
HM	–38.52(0.10)	35.20(1.10)	–3.32(1.10)	–11.3(0.08)	7.98(1.18)
QM	–28.71(0.10)	35.86(1.20)	7.15(1.30)	–12.8(0.04)	19.95(1.34)
AS	–38.91(0.10)	37.17(1.06)	–1.74(1.16)	–13.9(0.10)	12.16(1.26)
FL	–39.41(0.09)	37.35(1.04)	–2.06(1.13)	–14.9(0.09)	12.84(1.22)
DM	–46.70(0.08)	34.28(1.11)	–12.47(1.19)	–14.9(0.05)	2.43(1.24)
κ	0.62		0.56		
			50 × 1 ns		
WT	–47.79(0.06)	37.12(1.00)	–10.67(1.06)	–15.1(0.09)	4.43(1.15)
HM	–43.63(0.10)	34.95(0.98)	–8.68(1.08)	–11.3(0.08)	2.62(1.16)
QM	–44.40(0.10)	37.33(1.01)	–7.07(1.11)	–12.8(0.04)	5.73(1.15)
AS	–46.15(0.08)	39.17(1.01)	–6.98(1.09)	–13.9(0.10)	6.92(1.19)
FL	–47.95(0.07)	38.74(1.08)	–9.21(1.15)	–14.9(0.09)	5.69(1.24)
DM	–47.62(0.07)	36.87(1.06)	–10.75(1.13)	–14.9(0.05)	4.15(1.18)
κ	0.98		0.55		
			50 × 4 ns		
WT	–47.68(0.03)	36.74(0.49)	–10.94(0.52)	–15.1(0.09)	4.16(0.61)
HM	–42.86(0.05)	35.45(0.52)	–7.41(0.57)	–11.3(0.08)	3.89(0.65)
QM	–43.93(0.05)	36.35(0.51)	–7.58(0.56)	–12.8(0.04)	5.22(0.60)
AS	–45.75(0.04)	37.53(0.54)	–8.22(0.58)	–13.9(0.10)	5.68(0.68)
FL	–48.01(0.04)	38.08(0.50)	–9.93(0.54)	–14.9(0.09)	4.97(0.63)
DM	–47.37(0.03)	37.39(0.51)	–9.98(0.54)	–14.9(0.05)	4.92(0.59)
κ	0.98		0.89		
SAQ-WT	–44.20(0.04)	36.30(0.53)	–7.90(0.57)	–13.0(0.04)	5.10(0.61)

[a] Enthalpic and entropic components are also shown as well as correlation coefficients (κ) of each theoretically computed set with respect to the experimental data. Mean energies are in kcal/mol. Standard errors are shown in parentheses. [b] Experimental results are taken from Ohtaka et al.[6]

Absolute and Relative Binding Free Energies. Table 4 and Figure 7 show the results of the binding enthalpies and entropies and the overall binding free energies for all MDR systems using the 1 × 50, 50 × 1, and 50 × 4 ns ensemble trajectory approaches as well as corresponding experimental results from Ohtaka et al.[6] and using the correlation coefficients of each theoretically computed data set with these experimental results. All systems exhibit more positive binding free energies than that of the experimental result.

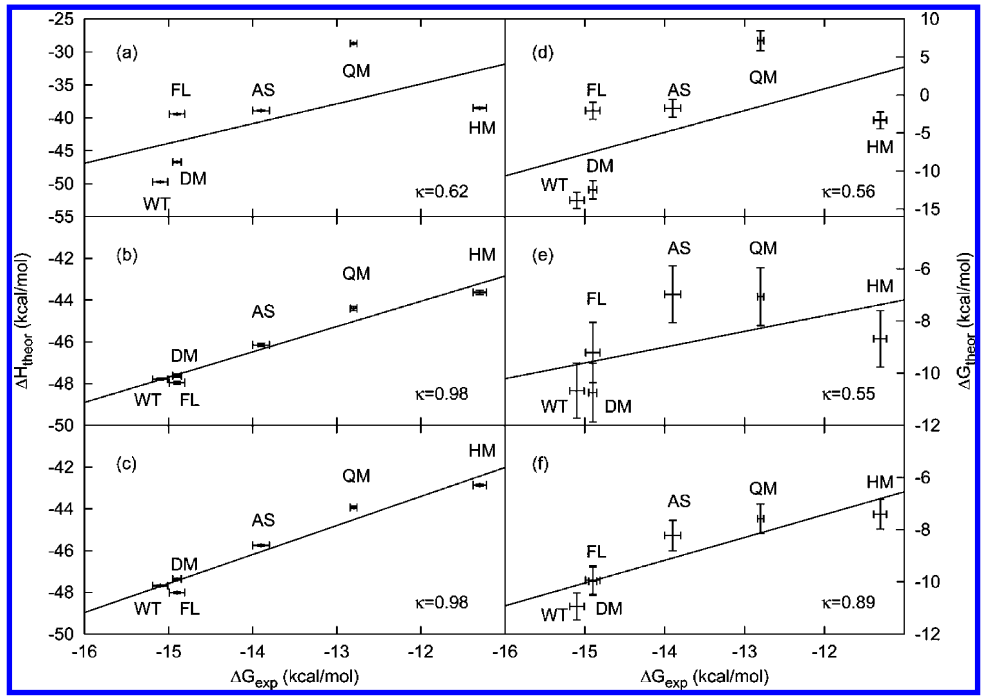

Figure 7. Experimental absolute binding free energies (ΔG_{exp}) of WT and MDR proteases (see Ohtaka et al.)[6] compared with theoretical predictions using binding free enthalpies (ΔH_{theor}) alone for the 1 × 50 ns, 50 × 1 ns and 50 × 4 ns trajectories in (a−c), respectively, and binding free energies (ΔG_{theor}) in (d−f), respectively. The correlation coefficient (κ) of each data set is also reported.

The 1 × 50 ns simulations exhibit large absolute deviations from the experimental result, indicative of inconsistent sampling. WT is within 1.2 kcal/mol of the experimental result. HM is nearly 8 kcal/mol more positive, while AS and FL systems are over 12 kcal/mol more positive. QM exhibits the largest deviation with a nearly 20 kcal/mol difference. By contrast, all 50 × 1 ns ensemble trajectories exhibit a smaller range of variation with respect to experiment (between 2.62 and 6.92 kcal/mol), indicative of a theoretically correctable systematic error. Furthemore, extension of the ensemble time scale to 50 × 4 ns further reduces the range of variation to between 3.89 and 5.68 kcal/mol from experiment.

Our results provide a rigorous assessment of same-state bound to same-state unbound proteases and exhibit a well confined deviation from experimental absolute binding free energies. The origin of this deviation arises from the various free energy terms that contribute to the state changes upon binding. In order to estimate the absolute binding free energy, we sum these various terms and compare with the deviation exhibited in our simulations. First, the β-hairpin flaps of the protease that mediate access to the active site change conformation from 'semiopen' to 'closed' upon binding. The semi-open unbound to closed unbound changes have been estimated in earlier picosecond studies to be on average ∼7 ± 3 kcal/mol;[34] individual results in the study varied from 2 ± 2 to 13 ± 5 kcal/mol. However, this average figure is physically unreasonable and is likely to be an overestimate. This is because flap changes are driven primarily by compensatory hydrophobic interactions. The glycine-rich flaps are composed of mainly hydrophobic residues. Conformational change from the semi-open to the closed state increases hydrophobic flap contacts with the opposite momomer at the expense of reduced contacts with the same monomer, and this compensation will present a significantly smaller free energy penalty than 7 kcal/mol. Recent calculations using explicit solvent aggregate μs-time scale ensemble molecular dynamics simulations have estimated the free energy of flap closure to be around 2.4 ± 0.4 kcal/mol,[70] in agreement with the lower estimate of Rick et al.[34]

Second, the unbound protease has different catalytic aspartyl protonation states depending on the bulk pH. Upon binding, the protease is considered to change from dianionic (at physiological pH) to become monoprotonated.[65] The free energy of this change has been estimated as a favorable 1−2 kcal/mol.[30] A final important contribution comes from explicit water-mediated protein−ligand interactions. A crucial tetrahedrally coordinated water molecule mediates favorable interactions in the flap−ligand cavity with a free energy contribution estimated between 3−3.5 kcal/mol in previous thermodynamic integration studies[35,36] and between 4−6 kcal/mol in structural refinement-based studies.[71] Summing these terms gives us a correction term of between 2−5.2 kcal/mol, in good agreement with the deviation of our results from the experimental binding free energies.

The large variation between the 1 × 50 and 50 × 1 ns trajectories is principally due to the inherent differences in binding enthalpy exhibited by the two methods. As mentioned in the previous section, these differences range from approximately 1−16 kcal/mol (see Table 4). Conversely, the 50 × 4 ns trajectory values are all within 1 kcal/mol of their respective 50 × 1 ns values, confirming that the 50 × 1 ns simulations are enthalpically converged and substantially improve sampling over the 1 × 50 ns trajectory method.

The configurational entropies for all systems are fairly similar where $-T\Delta S$ ranges between 34.28 to 37.35 kcal/mol in the 1 × 50 ns trajectories and 34.95 to 39.17 kcal/mol in the 50 × 1 ns trajectories. Furthermore, the largest entropic difference in the two methods between corresponding MDR proteases is 2 kcal/mol, exhibited by the AS system. This is slightly reduced between the two ensemble sets to 1.6 kcal/mol for the same system. This confirms that

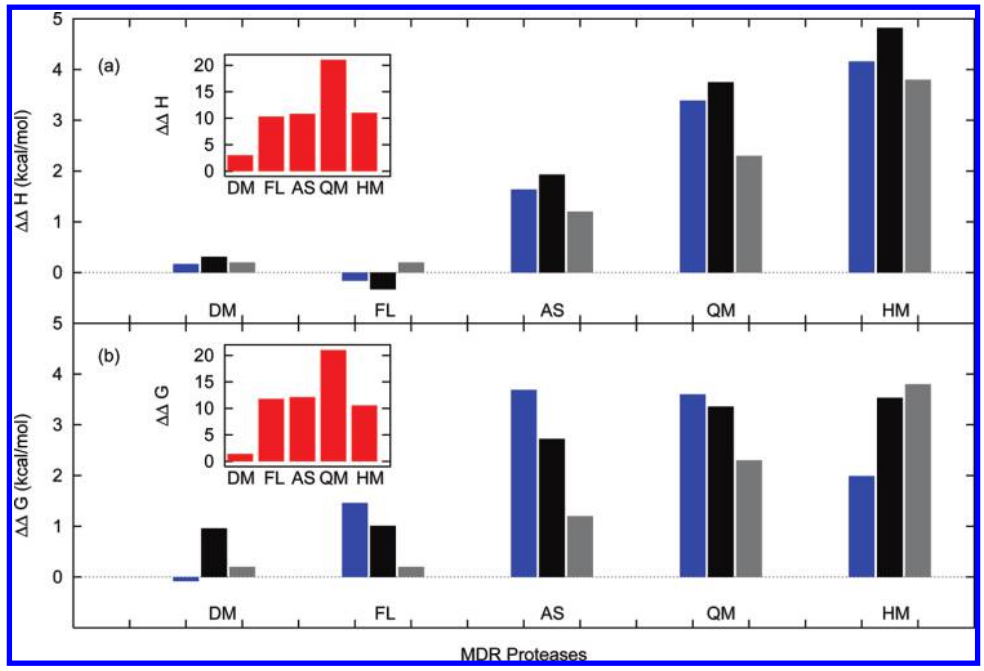

Figure 8. Theoretical vs experimental relative binding affinities of all mutant MDR proteases with respect to WT using differences in (a) binding free enthalpies alone and (b) binding free energies. The 1 × 50, 50 × 1, and 50 × 4 ns are represented by the red (inset), blue, and black bars, respectively, and compared to corresponding experimental (gray bars) differences (see Ohtaka et al.). [6] The ensemble approaches exhibit relative binding free energies that are much closer to experimental values.

for entropy the ensemble methodology does not significantly improve sampling beyond the single-trajectory method, while an increase in sampling within the ensemble method also makes no significant improvement to the result.

The greater the affinity between the inhibitor and a protease variant, the more negative the binding free energy. Mutation-induced loss of binding affinity, as compared to a wild-type protease, results in a less negative binding free energy. The relative binding free energy of a mutant with respect to the wild-type, defined as the difference between the absolute binding free energy of the mutant and the wild-type ($\Delta\Delta G = \Delta G_{mut} - \Delta G_{wt}$), is thus an important determinant of the degree of resistance conferred by a mutational variant.

Figure 8, and Table 1 in the Supporting Information, shows the relative binding free energies of all mutant MDR proteases with respect to WT using differences in the binding enthalpy alone and the binding free energy (Figure 8a and b, respectively), compared with corresponding experimental (gray bars) differences (see Ohtaka et al.).[6] The 1 × 50, 50 × 1, and 50 × 4 ns are represented by the red (inset), blue, and black bars, respectively.

First, based on relative binding free enthalpies, a correct ranking is achieved for all MDR mutants relative to the WT using the 1 × 50 ns approach, as all mutants exhibit more positive binding free enthalpies in line with experimental binding free energies. However, they are incorrectly ordered with respect to each other, for example, the QM system being ranked as substantially more resistant than all of the other systems, while the FL system is ranked as much more resistant than that of DM; experimentally they are equivalent.

Furthermore, the absolute differences are both much larger than and inconsistent with respect to experiment, being as large as 21 kcal/mol for the QM calculation as compared to an experimental difference of 2.3 kcal/mol, while only 3 kcal/mol larger for the DM system. This results in a low correlation coefficient with experiment of $\kappa = 0.62$ (see Figure 7). As the mutant systems do not exhibit similar deviations from experiment, these large discrepancies cannot be attributed to a systematic error and instead are explained by the poor enthalpic convergence exhibited by the FL, AS, and QM systems.

By contrast, relative binding free enthalpies (Figure 8a) obtained using the 50 × 1 ns approach are all far closer to the corresponding experimental values than the single-trajectory approach, in all cases lying within 1.1 kcal/mol of experiment. The DM system exhibits the closest relative free energy difference with only 0.03 kcal/mol difference to experiment. This is again attributable to the convergence properties of the ensemble approach. Here, good enthalpic convergence is exhibited by all systems, resulting in relative free enthalpies much closer to experiment. A correct ranking is exhibited for all mutants, except FL, relative to the WT and with respect to each other. The FL system is ranked as more favorable to binding than the WT but is within 0.4 kcal/mol of the experimental difference. Furthermore, the differences with respect to experiment are much more consistent, resulting in an overall correlation coefficient of $\kappa = 0.98$ (see Figure 7). The 50 × 4 ns method does not change the results qualitatively. The same correlation coefficient is exhibited, but the FL system is still ranked as more favorable than the WT. The excellent correlation coefficient is attributable to the well converged enthalpic component in the ensemble methodology.

Ranking based on relative binding free energies shows a decrease in the correlation coefficient across all sampling methods (see Figure 7). The correlation coefficient for the single-trajectory approach is $\kappa = 0.56$, a small deterioraton compared to using binding enthalpies. This is explained even further by the positive deviation of the FL and AS systems and by the reduced deviation of the HM with respect to the WT (Figure 8b). A significant deterioration of the correlation

Table 5. Decomposed Components of the Free Energy of Binding for Wild-Type and All MDR Proteases with Lopinavir As Well As Wild-Type with Saquinavir Using 50 × 4 ns Ensemble-Trajectory Runs[a]

sequence	ΔH_{vdw}	ΔH_{ele}	ΔH_{pol}^{sol}	ΔH_{nonpol}^{sol}	ΔH_{ele}^{tot}	ΔH_{theor}	$-T\Delta S_{theor}$
WT	−72.82(0.03)	−51.29(0.05)	84.56(0.05)	−8.13(0.00)	33.27(0.04)	−47.68(0.03)	36.74(0.49)
HM	−70.43(0.04)	−50.51(0.08)	86.17(0.06)	−8.10(0.00)	35.66(0.05)	−42.86(0.05)	35.45(0.52)
QM	−71.62(0.03)	−52.03(0.08)	87.88(0.06)	−8.15(0.00)	35.85(0.05)	−43.93(0.05)	36.35(0.51)
AS	−71.02(0.03)	−51.97(0.07)	85.38(0.05)	−8.13(0.00)	33.41(0.04)	−45.75(0.04)	37.53(0.54)
FL	−73.11(0.03)	−52.02(0.06)	85.26(0.05)	−8.14(0.00)	33.24(0.04)	−48.01(0.04)	38.08(0.50)
DM	−72.71(0.03)	−52.29(0.05)	85.76(0.05)	−8.13(0.00)	33.47(0.04)	−47.37(0.03)	37.39(0.51)
SAQ-WT	−75.79(0.03)	−49.18(0.06)	89.08(0.06)	−8.32(0.00)	39.91(0.04)	−44.20(0.04)	36.30(0.53)

[a] Mean energies are in kcal/mol. Standard errors are shown in parentheses.

coefficient from 0.98 to 0.55 is exhibited by the 50 × 1 ns method due to the reduced positive deviation of the HM system and the increased positive deviation of the QM and AS systems, both of which are ranked incorrectly as more resistant than HM.

By contrast, relative ranking using the 50 × 4 ns approach still yields an excellent correlation coefficient of $\kappa = 0.89$, only a minor deterioration from using binding enthalpies alone. Furthermore, every mutant is correctly ranked not only with respect to the WT system but also with respect to each other. The deviation from experiment of the relative binding free energy is within ∼1.1 kcal/mol for all systems, except for the AS system which is within 1.52 kcal/mol. The mean deviation from experiment is 0.9 kcal/mol.

The differences between the ranking properties of single and ensemble approaches when using both the relative binding enthalpies and the relative binding free energies are attributable to two factors. First, the difference in enthalpic convergence between single and ensemble methods and, second, the non-Gaussian sampling of configurational entropy attained by the normal mode method. The effect of the inherent accuracy limitations of the configurational entropy exhibited by both single and ensemble approaches have the effect of compounding the poor enthalpic convergence properties in the case of the single-trajectory simulations. In the ensemble simulations, the enthalpic component is very well converged, leading to excellent ranking. It is the limited accuracy of the entropy calculation which causes a deterioration in the ranking when using relative binding free energies in the 50 × 1 ns trajectories and not enthalpies alone. Increasing the sample time in the 50 × 4 ns method increases the accuracy of the entropy calculation accounting for the correction of ranking across all systems, albeit with a modest drop in correlation with respect to enthalpies.

These results, therefore, show that the enthalpic component of the MMPBSA calculation is more sensitive to sampling method than to sample size, requiring an ensemble method for accurate ranking. By contrast, the entropic component is more sensitive to the sample size than to sampling method, with entropic results not changing substantially between single and ensemble methods. Instead, because the accuracy of the entropic calculation using the normal mode method is limited, large sample sets are required to achieve a level that permits accurate relative ranking of drug resistant mutants which differ by 1−4 kcal/mol.

THERMODYNAMIC AND STRUCTURAL CORRELATES OF RANKING

In order to better understand the factors driving both the binding of lopinavir to wild-type HIV-1 protease in general and the increased resistance in the mutant proteases, we decomposed the binding thermodynamics of all MDR mutants using the converged 50 × 4 ns ensemble trajectories. Furthermore, in order to understand the thermodynamic factors which confer the experimentally observed increased binding affinity of lopinavir over the first generation inhibitor saquinavir, we compared the decomposed thermodynamic components of both inhibitors binding to wild-type HIV-1 protease.

MDR Protease−Lopinavir Ranking. Table 5 shows the results of the decomposition into van der Waals (ΔH_{vdw}), electrostatic (ΔH_{ele}), polar (ΔH_{pol}^{sol}) and nonpolar (ΔH_{nonpol}^{sol}) solvation components as well as the total binding enthalpy (ΔH_{theor}) and configurational entropy ($-T\Delta S_{theor}$) components. The binding of lopinavir to wild-type HIV-1 protease is characterized by overridingly favorable van der Waals interactions as large as −72.82 kcal/mol in the WT HIV-1 protease. These are compensated for partially by a net total electrostatic repulsion of 33.27 kcal/mol, composed of a favorable vacuum electrostatic interaction (−51.29 kcal/mol) and a repulsive polar solvation term (84.56 kcal/mol). An additionally favorable nonpolar solvation term (−8.13 kcal/mol) completes the total enthalpic contribution to binding which is −47.68 kcal/mol (see Table 5). Configurational entropy, while significant (36.74 kcal/mol), is not as large as the enthalpic component, resulting in a net favorable binding free energy.

Relative ranking of MDR proteases indicates that resistance, at least for strongly resistant mutants such as AS, QM and HM, is principally enthalpically driven. Care has to be taken in interpreting increased enthalpy as the primary cause of resistance for less resistant mutants, such as DM and FL. This is because of the limited accuracy of the configurational entropy results. It is possible that increased accuracy would allow differences in configurational entropy between mutants to be meaningfully discriminated. However, due to the small relative variation (up to 2.6 kcal/mol) of the configurational entropies across different mutants, it is in fact possible to draw meaningful discrimination between the enthalpic differences across most mutants.

The principal effects of the MDR mutations are to decrease the van der Waals component of binding by approximately 2.4 kcal/mol between WT and HM and to increase the net electrostatic repulsion by the same amount resulting in an aproximately 4.8 kcal/mol decreased binding enthalpy. This is attenuated slightly by the decreased change in configurational entropy which indicates a less dramatic decrease in flexibility upon binding. The same pattern is observed for the QM system with respect to the WT system, except to a slightly lesser extent with respect to van der Waals interac-

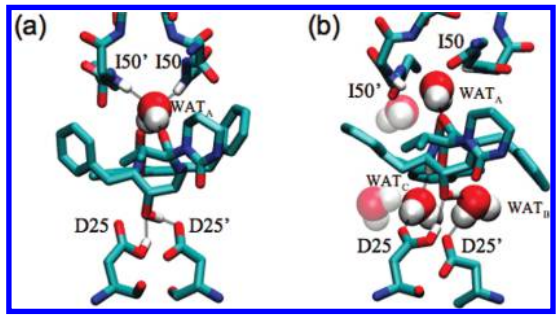

Figure 9. Conformations of direct and water-mediated hydrogen-bond interactions in the active site of the HM mutant with lopinavir bound for (a) the energy minimized initial structure and (b) a snapshot showing representative water-mediated alteration of the hydrogen-bond network in the 50 × 4 ns ensemble. Flap−ligand hydrogen-bond-mediating water molecules are labeled WAT_A, WAT_B, and WAT_C, additional water moelcules not mediating hydrogen-bond interactions are transparently displayed. Hydrogen bonds are displayed by black lines.

tions. The AS system exhibits the largest stepwise decrease in van der Waals interaction out of the three pairwise mutations. This can be explained by the directly reduced hydrophobic interaction induced by the V82A/I84V mutation. Interestingly, the FL system has a more favorable van der Waals interaction which is compensated by an increased change in configurational entropy, while DM has less favorable van der Waals interactions and less repulsive electrostatic interactions as well as moderately increased changes in configurational entropy. However, the changes in DM and FL cannot be interpreted as causing increased resistance due to the marginal decrease in binding free energy being cloaked by the uncertainty in the configurational entropy.

Observation of the propensity of water molecules to enter the active site during the course of the simulation reveals insights into additional structural correlates of MDR resistance. The population density of water molecules entering the active site cavity region was calculated for each of the six protease−lopinavir systems based on a water occupancy in the catalytic region defined by a radius of 3 Å from the catalytic dyad. This yields a correlation coefficient of 0.89 and 0.99 with respect to the calculated binding free energies and experimental binding free energies, respectively, (see Table 2 in the Supporting Information) indicating that water plays a significant structural role in causing resistance.

Figure 9a and b shows snapshots of a minimized initial structure and a conformation representing water entry for the HM system, respectively. In the initial structure (Figure 9a) the inter flap−ligand water molecule (WAT_A) is the only one in the active site and is tetrahedrally hydrogen bonded with residues I50/I50′ and lopinavir. The monoprotonated D25/D25′ dyad exhibits two strong hydrogen bonds with the hydroxyethylene moiety of lopinavir. Water occupancy in the catalytic region disrupts the hydrogen-bond network between the hydroxyethylene moiety of lopinavir and the monoprotonated D25/D25′ residues. In this conformation (Figure 9b), D25 maintains its hydrogen bond, but entry of a water molecule WAT_B disrupts direct D25′ hydrogen bonding. Instead, WAT_B mediates interactions between D25′ and the hydroxyethylene moiety of lopinavir by hydrogen bonding to both. A further catalytic cavity-entered water molecule, WAT_C, mediates interactions between D25 and the backbone amide of lopinavir. Additional waters that come within 3 Å of both protein and ligand but do not mediate inter-protein−ligand interactions are shown in transparency.

This alteration in the hydrogen-bond network may explain the increasing electrostatic repulsion exhibited in the MMPBSA calculation for the MDR mutants. Increased water occupancy indicates that the shape and size of the active site for MDR mutants differs significantly to that of the WT. Geometrical distortions of the binding site have recently been reported for the V82F/I84V mutant,[62] which is very similar to the AS mutant investigated here. In the case of the MDR mutants, an increase in active site volume induced by structural rearrangements of the mutations would explain both the increased water occupancy as well as the progressive decrease in inhibitor binding.

Cross-Drug Thermodynamic Ranking. In order to test whether the method developed here is capable of accurately ranking different inhibitors binding to the protease, we calculated the binding free energy of saquinavir to wild-type protease (from the 1FB7 crystal structure) using the 50 × 4 ns ensemble method and compared to lopinavir binding to the wild-type.

The binding free energy of saquinavir to wild-type HIV-1 protease together with the enthalpic, entropic, and decomposed values are shown in Tables 4 and 5. The absolute binding free energy is calculated as −7.9 kcal/mol, giving a 5.1 kcal/mol more positive value than experiment, which is consistent with the deviations of all other mutants from their respective experimental values and can thus also be attributed to a systematic error. Experimentally, saquinavir binds less well to WT than lopinavir by 2.1 kcal/mol. Our calculations give a value of 3.04 kcal/mol, in good agreement with experiment, and are thus able to rank the two inhibitors correctly within 1 kcal/mol of the experimental difference. Furthermore, analysis of the decomposed thermodynamics explains the origin of the increased binding free energy of lopinavir as being enthalpically driven. The enthalpic component of binding is 3.48 kcal/mol more favorable for lopinavir. This originates from a much smaller net electrostatic repulsion than saquinavir, 33.27 kcal/mol compared to 39.91 kcal/mol, which is only partially compensated by a more favorable van der Waals interaction for saquinavir, −75.79 kcal/mol compared to −72.82 kcal/mol. The overall change in configurational entropy is similar for both systems, suggesting a similar flexibility change upon binding.

These results suggest that improved drug design should focus on increasing the van der Waals interactions while simultaneously decreasing the net electrostatic repulsion upon binding. Unfortunately, optimizing the net electrostatic interaction is nontrivial because the greater the direct electrostatic interactions between inhibitor and protein, the more likely the increase in polar solvation penalty. Lopinavir's decreased electrostatic penalty is attributable to both increased favorable electrostatic interactions coupled with a smaller polar solvation penalty. Indeed, the resistance exhibited by the HM mutant is partially attributable to this concerted effect and suggests that multidrug-resistant mutants may also use this mechanism to confer resistance, possibly through the disruption of key protease−inhibitor interactions by water molecules, as discussed earlier.

CONCLUSIONS

We show that ensemble molecular dynamics approaches herald a significantly enhanced way of sampling accurate and converged relative binding free energies of biomolecular structures compared with single-trajectory approaches. We perform molecular mechanics Poisson−Boltzmann surface area (MMPBSA) and configurational entropy-based free energy calculations using fully atomistic molecular dynamics (MD) simulations[16,39] of multidrug-resistant (MDR) HIV-1 proteases bound to lopinavir on an unprecedented scale. These show that single-trajectory systems are prone to become trapped in local minima thus precluding correct Gaussian sampling expected from independent estimates of free energy. Configurational entropies calculated using normal-mode analysis do not exhibit normal distributions by either the single or the ensemble approaches even after exhaustive sampling (1000 snapshots). Instead, entropies are grouped around several distinct peaks most likely due to the reduction of available conformations after minimization in the normal-mode procedure.[69]

The ensemble approach yields accurate results even with approximate methods, like MMPBSA, and elucidates the molecular determinants of resistance in HIV-1 protease. Using differences in binding free energies, completely correct ranking is obtained for six HIV-1 protease variants with a correlation coefficient of 0.89 and a mean relative deviation from experiment of only 0.9 kcal/mol. MDR resistance to lopinavir is enthalpically driven and increases both by a decrease in the protein−ligand van der Waals interaction of up to 2.5 kcal/mol, principally due to the V82A/I84V (AS) mutant, and by an increase in the net electrostatic repulsion of up to 2.5 kcal/mol, due to water-mediated disruption of protein−ligand interactions. Our method also successfully distinguishes the potency of lopinavir over the first-generation inhibitor saquinavir in good agreement with experiment. Both lopinavir and saquinavir bind principally due to favorable van der Waals interactions. However, lopinavir's increased potency is due to a substantially smaller electrostatic repulsion upon binding, even though saquinavir exhibits a larger van der Waals interaction. Improved drug design should, therefore, focus specifically on reducing the net electrostatic repulsion upon binding, while maintaining a strong van der Waals interaction.

Our findings suggest a limiting accuracy in the normal-mode approach to calculating configurational entropies. Such limitations may or may not be a factor in future determination of relative binding free energies using the MMPBSA/configurational entropy method. It is likely that other methods, such as quasiharmonic analysis, that do not result in a reduction of available conformations and that instead rely on components within a large set of conformational states may prove to be more effective than the normal-mode approach when compared with the MMPBSA method. In general, therefore, for related molecular systems which may exhibit significant changes in entropy, success in ranking depends on accurate determination of configurational entropies.

Determination of accurate absolute binding free energies remains an outstanding problem in computational biochemistry. End-state methods, like MMPBSA, do not account for additional thermodynamic changes upon binding, such as conformational changes, protonation state changes, and water mediated interactions. Therefore, the optimal outcome for the MMPBSA method is to achieve binding free energies within the summed contribution of these additional factors. Such factors have been investigated for the HIV-1 protease,[33−36] and summing them, specifically the thermodynamic penalty to binding from flap-conformational changes with favorable interactions due to protonation state changes and water interactions, could yield an additionally favorable interaction of between 2−5.2 kcal/mol upon binding. Our findings are in excellent agreement with such a correction term, all converged trajectories exhibiting between 3.9−5.7 kcal/mol positive deviation from the absolute experimental binding free energy.

However, although such agreement demonstrates that our method provides accurate calculation of same-state bound to same-state unbound absolute binding free energies for HIV-1 protease−ligand complexes, provided suitable convergence has been reached, care has to be taken when interpreting the overall relative binding free energies. This is because the correction term which accounts for the free energy difference of the changing state upon binding may vary from one protease sequence to another. Such differences, however, are likely to be either small or at least compensatory, as otherwise they would lead to much larger experimental free energy differences. Indeed, the reproducibility exhibited by our study suggests that such small mutation-dependent state change variations may also partially account for the slight discrepancies between the experimental and the calculated relative binding free energies reported here.

Recent investigations which applied the metadynamics approach reported moderately accurate binding free energies of a small peptide to HIV-1 protease using biased direct association over a simulation time of 1.6 μs.[37] It would be interesting to see whether such methods are also capable of effective ranking of multiple protein−ligand combinations in the future, especially larger peptides and/or inhibitors. Convergence of the MMPBSA and entropic contributions to binding for these systems requires up to 200 ns of fully atomistic sampling per system. It is likely that our investigation thus reaches the computational limit of thermodynamic end-state models, beyond which alternative methodologies become increasingly desirable. Furthermore, our investigations suggest that ensemble MD coupled to the MMPBSA calculation method used here may be sufficient to confer the discrimination of binding affinities within 1 kcal/mol of each other, saving a computational cost of 1 order of magnitude.

Theoretical minimum wallclock turn-around time for the entire study is as fast as three days using 9600 cores on Ranger, including postproduction analysis. Since accurate methods that discriminate mutant HIV-1 protease−ligand binding affinities are expected to play a significant role in conferring patient-specific support in clinical decision making,[38] for which wallclock time is of principal concern, our study promotes rapid and accurate ranking of HIV-1 protease−ligand binding free energies for optimizing patient-specific treatment.

ACKNOWLEDGMENT

We thank Dr. Simon Watson and Dr. Simon Clifford for assistance and Prof. Ian Ford for discussions. We are grateful

to EPSRC and CoMPLEX for funding the Ph.D. studentships of D.W.W. and O.A.K. We are also grateful to EPSRC for funding much of this research through RealityGrid grant GR/R67699. Our work was partially supported by the National Science Foundation under NRAC grant MCA04N014, utilizing the Ranger machine at the Texas Advanced Computing Center (TACC). We also wish to thank the U.K. NGS for providing access to their resources. This research has been partially supported by the EU FP6-funded ViroLab project (IST-027446).

Supporting Information Available: Enthalpic and entropic running average and cumulative mean binding data, RMSD structural flexibility analysis, relative binding free energies, and water occupancy correlation to binding free energy. This information is available free of charge via the Internet at http://pubs.acs.org.

REFERENCES AND NOTES

(1) Ohtaka, H.; Muzammil, S.; Schon, A.; Velazquez-Campoy, A.; Vega, S.; Freire, E. Thermodynamic rules for the design of high affinity HIV-1 protease inhibitors with adaptability to mutations and high selectivity towards unwanted targets. *Int. J. Biochem. Cell Biol.* **2004**, *36*, 1787–1799.

(2) Velazquez-Campoy, A.; Luque, I.; Todd, M. J.; Milutinovich, M.; Kiso, Y.; Freire, E. Thermodynamic dissection of the binding energetics of KNI-272, a potent HIV-1 protease inhibitor. *Protein Sci.* **2000**, *9*, 1801–1809.

(3) Maschera, B.; Darby, G.; Palu, G.; Wright, L. L.; Tisdale, M.; Myers, R.; Blair, E. D.; Furfine, E. S. Human immunodeficiency virus: Mutations in the viral protease that confer resistance to saquinavir increase the dissociation rate constant of the protease-saquinavir complex. *J. Biol. Chem.* **1996**, *271*, 33231–33235.

(4) Ermolieff, J.; Lin, X.; Tang, J. Kinetic properties of saquinavir-resistant mutants of human immunodeficiency virus type 1 protease and their implications in drug resistance in Vivo. *Biochemistry* **1997**, *36*, 12364–12370.

(5) Ohtaka, H.; Velazquez-Campoy, A.; Xie, D.; Freire, E. Overcoming drug resistance in HIV-1 chemotherapy: The binding thermodynamics of amprenavir and TMC-126 to wild-type and drug resistant mutants of the HIV-1 protease. *Protein Sci.* **2002**, *11*, 1908–1916.

(6) Ohtaka, H.; Schon, A.; Freire, E. Multidrug resistance to HIV-1 protease inhibition requires cooperative coupling between distal mutations. *Biochemistry* **2003**, *42*, 13659–13666.

(7) Wang, W.; Donini, O.; Reyes, C. M.; Kollman, P. A. Biomolecular simulations: Recent developments in force fields, simulations of enzyme catalysis, protein-ligand, protein-protein, and protein-nucleic acid noncovalent interactions. *Annu. Rev. Biophys. Biomol. Struct.* **2001**, *30*, 211–243.

(8) Aqvist, J.; Medina, C.; Samuelsson, J.-E. A new method for predicting binding affinity in computer-aided drug design. *Protein Eng.* **1994**, *7*, 385–391.

(9) Chen, X.; Weber, I. T.; Harrison, R. W. Molecular dynamics simulations of 14 HIV protease mutants in complexes with indinavir. *J. Mol. Model.* **2004**, *10*, 373–381.

(10) Rick, S. W.; Topol, I. A.; Erickson, J. W.; Burt, S. K. Molecular mechanisms of resistance: Free energy calculations of mutation effects on inhibitor binding to HIV-1 protease. *Protein Sci.* **1998**, *7*, 1750–1756.

(11) Fowler, P. W.; Geroult, S.; Jha, S.; Waksman, G.; Coveney, P. V. Rapid and accurate calculation of relative binding affinities for the SH2 domain using a computational grid. *J. Chem. Theory Comput.* **2007**, *3*, 1193–1202.

(12) Woo, H.-J.; Roux, B. Calculation of absolute protein-ligand binding free energy from computer simulations. *Proc. Natl. Acad. Sci. U.S.A.* **2005**, *102*, 6825–6830.

(13) Kollman, P. A.; Massova, I.; Reyes, C.; Kuhn, B.; Huo, S.; Chong, L.; Lee, M.; Lee, T.; Duan, Y.; Wang, W.; Donini, O.; Cieplak, P.; Srinivasan, J.; Case, D. A.; Cheatham, T. E. r. Calculating structures and free energies of complex molecules: combining molecular mechanics and continuum models. *Acc. Chem. Res.* **2000**, *33*, 889–897.

(14) Wang, W.; Kollman, P. A. Computational study of protein specificity: The molecular basis of HIV-1 protease drug resistance. *Proc. Natl. Acad. Sci. U.S.A.* **2001**, *98*, 14937–14942.

(15) Wan, S.; Coveney, P. V.; Flower, D. R. Peptide recognition by the T cell receptor: Comparison of binding free energies from thermodynamic integration, Poisson-Boltzmann and linear interaction energy approximations. *Phil. Trans. R. Soc., A* **2005**, *363*, 2037–2053.

(16) Stoica, I.; Sadiq, S. K.; Coveney, P. V. Rapid and accurate prediction of binding free energies of saquinavir-bound HIV-1 proteases. *J. Am. Chem. Soc.* **2008**, *130*, 2639–2648.

(17) Caves, L. S. D.; Evanseck, J. D.; Karplus, M. Locally accessible conformations of proteins: Multiple molecular dynamics simulations of crambin. *Protein Sci.* **1998**, *7*, 649–666.

(18) Shirts, M.; Pande, V. S. Computing: Screen Savers of the World Unite. *Science* **2000**, *290*, 1903–1904.

(19) Jayachandran, G.; Vishal, V.; Pande, V. S. Using massively parallel simulation and Markovian models to study protein folding: examining the dynamics of the villin headpiece. *J. Chem. Phys.* **2006**, *124*, 164902.

(20) Kasson, P. M.; Kelley, N. W.; Singhal, N.; Vrljic, M.; Brunger, A. T.; Pande, V. S. Ensemble molecular dynamics yields submillisecond kinetics and intermediates of membrane fusion. *Proc. Natl. Acad. Sci. U.S.A.* **2006**, *103*, 11916–11921.

(21) Jayachandran, G.; Shirts, M. R.; Park, S.; Pande, V. S. Parallelized-over-parts computation of absolute binding free energy with docking and molecular dynamics. *J. Chem. Phys.* **2006**, *125*, 084901.

(22) Fujitani, H.; Tanida, Y.; Ito, M.; Jayachandran, G.; Snow, C. D.; Shirts, M. R.; Sorin, E. J.; Pande, V. S. Direct calculation of the binding free energies of FKBP ligands. *J. Chem. Phys.* **2005**, *123*, 084108.

(23) Zoete, V.; Michielin, O.; Karplus, M. Relation between sequence and structure of HIV-1 protease inhibitor complexes: A model system for the analysis of protein flexibility. *J. Mol. Biol.* **2002**, *315*, 21–52.

(24) Layten, M.; Hornak, V.; Simmerling, C. The open structure of a multi-drug-resistant HIV-1 protease is stabilized by crystal packing contacts. *J. Am. Chem. Soc.* **2006**, *128*, 13360–13361.

(25) Sadiq, S. K.; Wan, S.; Coveney, P. V. Insights into a mutation-assisted lateral drug escape mechanism from the HIV-1 protease active site. *Biochemistry* **2007**, *46*, 14865–14877.

(26) Hornak, V.; Okur, A.; Rizzo, R. C.; Simmerling, C. HIV-1 protease flaps spontaneously open and reclose in molecular dynamics simulations. *Proc. Natl. Acad. Sci. U.S.A.* **2006**, *103*, 915–920.

(27) Hornak, V.; Okur, A.; Rizzo, R. C.; Simmerling, C. HIV-1 protease flaps spontaneously close to the correct structure in simulations following manual placement of an inhibitor into the open state. *J. Am. Chem. Soc.* **2006**, *128*, 2812–2813.

(28) Toth, G.; Borics, A. Closing of the flaps of HIV-1 protease induced by substrate binding: A model of a flap closing mechanism in retroviral aspartic proteases. *Biochemistry* **2006**, *45*, 6606–6614.

(29) Toth, G.; Borics, A. Flap opening mechanism of HIV-1 protease. *J. Mol. Graphics Modell.* **2006**, *24*, 465–474.

(30) Wittayanarakul, K.; Hannongbua, S.; Feig, M. Accurate prediction of protonation state as a prerequisite for reliable MM-PB(GB)SA binding free energy calculations of HIV-1 protease inhibitors. *J. Comput. Chem.* **2008**, *29*, 673–685.

(31) Wlodawer, A.; Erickson, J. W. Structure-based inhibitors of HIV-1 Protease. *Annu. Rev. Biochem.* **1993**, *62*, 543–585.

(32) Wang, Y.-X.; Freedberg, D. I.; Wingfield, P. T.; Stahl, S. J.; Kaufman, J. D.; Kiso, Y.; Bhat, T. N.; Erickson, J. W.; Torchia, D. A. Bound Water Molecules at the Interface between the HIV-1 Protease and a Potent Inhibitor, KNI-272, Determined by NMR. *J. Am. Chem. Soc.* **1996**, *118*, 12287–12290.

(33) Lepsik, M.; Kriz, Z.; Havlas, Z. Efficiency of a second-generation HIV-1 protease inhibitor studied by molecular dynamics and absolute binding free energy calculations. *Proteins: Struct., Funct., Bioinf.* **2004**, *57*, 279–293.

(34) Rick, S. W.; Erickson, J. W.; Burt, S. K. Reaction path and free energy calculations of the transition between alternate conformations of HIV-1 protease. *Proteins: Struct., Funct., Genet.* **1998**, *32*, 7–16.

(35) Hamelberg, D.; McCammmon, J. A. Standard free energy of releasing a localized water molecule from the binding pockets of proteins: Double-decoupling method. *J. Am. Chem. Soc.* **2004**, *126*, 7683–7689.

(36) Lu, Y.; Yang, C.-Y.; Wang, S. Binding free energy contributions of interfacial waters in HIV-1 protease/inhibitor complexes. *J. Am. Chem. Soc.* **2006**, *128*, 11830–11839.

(37) Pietrucci, F.; Marinelli, F.; Carloni, P.; Laio, A. Substrate binding mechanism of HIV-1 protease from explicit-solvent atomistic simulations. *J. Am. Chem. Soc.* **2009**, *131*, 11811–11818.

(38) Sadiq, S. K.; Mazzeo, M. D.; Zasada, S. J.; Manos, S.; Stoica, I.; Gale, C. V.; Watson, S. J.; Kellam, P.; Brew, S.; Coveney, P. V. Patient-specific simulation as a basis for clinical decision-making. *Phil. Trans. R. Soc., A* **2008**, *366*, 3199–3219.

(39) Sadiq, S. K.; Wright, D.; Watson, S. J.; Zasada, S. J.; Stoica, I.; Coveney, P. V. Automated molecular simulation based binding affinity calculator for ligand-bound HIV-1 proteases. *J. Chem. Inf. Model.* **2008**, *48*, 1909–1919.

(40) Sloot, P.; Coveney, P.; Bubak, M. T.; Vandamme, A.-M.; O Nuallain, B.; van de Vijver, D.; Boucher, C. Multi-Science Decision Support for HIV Drug Resistance Treatment. *Stud. Health. Technol. Inform* **2008**, *138*, 188–198.
(41) Stoica, I.; Sadiq, S. K.; Gale, C. V.; Coveney, P. V. Virtual Physiological Human research initiative: the future for rational HIV treatment design? *Future HIV Ther.* **2008**, *2*, 419–425.
(42) Sloot, P. M. A.; Coveney, P. V.; Ertaylan, G.; Muller, V.; Boucher, C. A.; Bubak, M. HIV decision support: from molecule to man. *Phil. Trans. R. Soc., A* **2009**, *367*, 2691–2703.
(43) Wu, T. D.; Schiffer, C. A.; Gonzales, M.; Taylor, J.; Kantor, R.; Chou, S.; Israelski, D.; Zolopa, A. R.; Fessel, W. J.; Shafer, R. W. Mutation patterns and structural correlates in human immunodeficiency virus type 1 protease following different protease inhibitor treatments. *J. Virol.* **2003**, *77*, 4836–4847.
(44) Svicher, V.; Ceccherini-Silberstein, F.; Erba, F.; Santoro, M.; Gori, C.; Bellochi, M. C.; Giannella, S.; Trotta, M. P.; d'Arminio Monforte, A.; Antinori, A.; Perno, C. F. Novel human immunodeficiency virus type 1 protease mutations potentially involved in resistance to protease inhibitors. *Antimicrob. Agents Chemother.* **2005**, *49*, 2015–2025.
(45) Johnson, V. A.; Brun-Vezinet, F.; Clotet, B.; Conway, B.; Kuritzkes, D. R.; Pillay, D.; Schapiro, J.; Richman, D. Update of the drug resistance mutations in HIV-1: Fall 2006. *J. Int. AIDS Soc.* **2006**, *14*, 125–130.
(46) Coveney, P. V.; Saksena, R. S.; Zasada, S. J.; McKeown, M.; Pickles, S. The application hosting environment: Lightweight middleware for grid-based computational science. *Comput. Phys. Commun.* **2007**, *176*, 406–418.
(47) Schuettelkopf, A. W.; van Aalten, D. M. F. PRODRG - a tool for high-throughput crystallography of protein-ligand complexes. *Acta Crystallogr., Sect. D: Biol. Crystallogr.* **2004**, *60*, 1355–1363.
(48) Frisch, M. J.; Trucks, G. W.; Schlegel, H. B.; Scuseria, G. E.; Robb, M. A.; Cheeseman, J. R.; Montgomery, J. A., Jr.; Vreven, T.; Kudin, K. N.; Burant, J. C.; Millam, J. M.; Iyengar, S. S.; Tomasi, J.; Barone, V.; Mennucci, B.; Cossi, M.; Scalmani, G.; Rega, N.; Petersson, G. A.; Nakatsuji, H.; Hada, M.; Ehara, M.; Toyota, K.; Fukuda, R.; Hasegawa, J.; Ishida, M.; Nakajima, T.; Honda, Y.; Kitao, O.; Nakai, H.; Klene, M.; Li, X.; Knox, J. E.; Hratchian, H. P.; Cross, J. B.; Bakken, V.; Adamo, C.; Jaramillo, J.; Gomperts, R.; Stratmann, R. E.; Yazyev, O.; Austin, A. J.; Cammi, R.; Pomelli, C.; Ochterski, J. W.; Ayala, P. Y.; Morokuma, K.; Voth, G. A.; Salvador, P.; Dannenberg, J. J.; Zakrzewski, V. G.; Dapprich, S.; Daniels, A. D.; Strain, M. C.; Farkas, O.; Malick, D. K.; Rabuck, A. D.; Raghavachari, K.; Foresman, J. B.; Ortiz, J. V.; Cui, Q.; Baboul, A. G.; Clifford, S.; Cioslowski, J.; Stefanov, B. B.; Liu, G.; Liashenko, A.; Piskorz, P.; Komaromi, I.; Martin, R. L.; Fox, D. J.; Keith, T.; Al-Laham, M. A.; Peng, C. Y.; Nanayakkara, A.; Challacombe, M.; Gill, P. M. W.; Johnson, B.; Chen, W.; Wong, M. W.; Gonzalez, C.; Pople, J. A. *Gaussian 03*, revision C.02; Gaussian, Inc.: Wallingford, CT, 2004.
(49) Case, D. A.; Cheatham, T.; Darden, T.; Gohlke, H.; Luo, R.; Merz, K. M., Jr.; Onufriev, A.; Simmerling, C.; Wang, B.; Woods, R. The Amber biomolecular simulation programs. *J. Comput. Chem.* **2005**, *26*, 1668–1688.
(50) Humphrey, W.; Dalke, A.; Schulten, K. VMD - Visual molecular dynamics. *J. Mol. Graphics* **1996**, *14*, 33–38.
(51) Wang, J.; Wolf, R. M.; Case, D. A.; Kollman, P. A. Development and testing of a general AMBER force field (GAFF). *J. Comput. Chem.* **2004**, *25*, 1157–1174.
(52) Duan, Y.; Wu, C.; Chowdhury, S.; Lee, M. C.; Xiong, G.; Zhang, W.; Yang, R.; Cieplak, P.; Luo, R.; Lee, T. A point-charge force field for molecular mechanics simulations of proteins based on condensed-phase quantum mechanical calculations. *J. Comput. Chem.* **2003**, *24*, 1999–2012.
(53) Wlodawer, A.; Vondrasek, J. Inhibitors of HIV-1 protease: A major success of structure-assissted drug design. *Annu. Rev. Biophys. Biomol. Struct.* **1998**, *27*, 249–284.
(54) Schafmeister, C. E. A. F.; Ross, W. S.; Romanovski, V. *LEaP*; University of California: San Francisco, CA, 1995.
(55) Jorgensen, W. L.; Chandrasekhar, J.; Madura, J. D.; Impey, R. W.; Klein, M. L. Comparison of simple potential functions for simulating liquid water. *J. Chem. Phys.* **1983**, *79*, 926–935.
(56) Kale, L.; Skeel, R.; Bhandarkar, M.; Brunner, R.; Gursoy, A.; Krawetz, N.; Phillips, J.; Shinozaki, A.; Varadarajan, K.; Schulten, K. NAMD2: Greater scalability for parallel molecular dynamics. *J. Comput. Phys.* **1999**, *151*, 283–312.
(57) Essmann, U.; Perera, L.; Berkowitz, M. L.; Darden, T. A smooth particle mesh Ewald method. *J. Chem. Phys.* **1995**, *103*, 8577–9593.
(58) Ryckaert, J. P.; Ciccotti, G.; Berendsen, H. J. C. Numerical integration of the Cartesian equations of motion of a system with constraints: Molecular dynamics of n-alkanes. *J. Comput. Phys.* **1977**, *23*, 327–341.
(59) Berendsen, H. J. C.; Postma, J. P. M.; van Gunsteren, W. F.; DiNola, A.; Haak, J. R. Molecular dynamics with coupling to an external bath. *J. Chem. Phys.* **1984**, *81*, 3684–3690.
(60) Meagher, K. L.; Carlson, H. A. Solvation Influences Flap Collapse in HIV-1 Protease. *Proteins: Struct., Funct., Bioinf.* **2005**, *58*, 119–125.
(61) Sanner, M. F.; Olson, A. J.; Spehner, J. C. Reduced surface: an efficient way to compute molecular surfaces. *Biopolymers* **1996**, *38*, 305–320.
(62) Hou, T.; Yu, R. Molecular dynamics and free energy studies on the wild-type and double mutant HIV-1 protease complexed with amprenavir and two amprenavir-related inhibitors: mechanism for binding and drug resistance. *J. Med. Chem.* **2007**, *50*, 1177–1188.
(63) Wittayanarakul, K.; Aruksakunwong, O.; Sompornpisut, P.; Sanghiran-Lee, V.; Parasuk, V.; Pinitglang, S.; Hannongbua, S. Structure, dynamics and solvation of HIV-1 protease/saquinavir complex in aqueous solution and their contributions to drug resistance: Molecular dynamic simulations. *J. Chem. Inf. Model.* **2005**, *45*, 300–308.
(64) Sitkoff, D.; Sharp, K. A.; Honig, B. Accurate calculation of hydration free-energies using macroscopic solvent models. *J. Phys. Chem.* **1994**, *98*, 1978–1988.
(65) Kovalskyy, D.; Dubyna, V.; Mark, A. E.; Korenelyuk, A. A molecular dynamics study of the structural stability of HIV-1 protease under physiological conditions: The role of Na+ ions in stabilizing the active site. *Proteins: Struct., Funct., Bioinf.* **2005**, *58*, 450–458.
(66) Hyland, L. J.; Tomaszek, T. A., Jr.; Meek, T. D. Human immunodeficiency virus-1 protease. 2. Use of pH rate studies and solvent kinetic isotope effects to elucidate details of chemical mechanism. *Biochemistry* **1991**, *30*, 8454–8463.
(67) Harte, W. E., Jr.; Beveridge, D. L. Prediction of the protonation state of the active site aspartyl residues in HIV- 1 protease-inhibitor complexes via molecular dynamics simulation. *J. Am. Chem. Soc.* **1993**, *115*, 3883–3886.
(68) Andricioaei, I.; Karplus, M. On the calculation of entropy from covariance matrices of the atomic fluctuations. *J. Chem. Phys.* **2001**, *115*, 6289–6292.
(69) Brooks, B. R.; Janezic, D.; Karplus, M. Harmonic analysis of large systems. I. Methodology. *J. Comput. Chem.* **1995**, *16*, 1522–1542.
(70) Sadiq, S. K.; De Fabritiis, G. Explicit solvent dynamics and energetics of HIV-1 protease flap-opening and closing, preprint.
(71) Fornabaio, M.; Spyrakis, F.; Mozzarelli, A.; Cozzini, P.; Abraham, D.; Kellogg, G. Simple, Intuitive Calculations of Free Energy of Binding for Protein- Ligand Complexes. 3. The Free Energy Contribution of Structural Water Molecules in HIV-1 Protease Complexes. *J. Med. Chem.* **2004**, *47*, 4507–4516.

CI100007W